

TWO-DIMENSIONAL ANALYSIS OF MHD GENERATORS  
WITH SEGMENTED ELECTRODES

Z.N. Celinski and F.W. Fischer

IPP 3/26

Jan. 1965

**I N S T I T U T F Ü R P L A S M A P H Y S I K**

**G A R C H I N G B E I M Ü N C H E N**

# INSTITUT FÜR PLASMAPHYSIK

GARCHING BEI MÜNCHEN

IPP 3/26

Z.N. Celinski  
F.W. Fischer

Two-Dimensional Analysis of MHD  
Generators with Segmented Electrodes,  
January 1965 (in English)

## TWO-DIMENSIONAL ANALYSIS OF MHD GENERATORS WITH SEGMENTED ELECTRODES

Z.N. Celinski and F.W. Fischer

ABSTRACT

The distribution of electrical parameters in MHD  
generators was determined by numerical methods for  
any channel geometry and any practical Hall parameter.  
The analysis was limited to generators with a separate  
electrical circuit for each pair of electrodes. Constant  
gas dynamic parameters and constant generator cross-section  
were assumed. A correction factor  $\lambda$  was calculated, the  
use of which makes it possible to correct one-dimensional  
theory equations for two-dimensional effects. Optimum  
electrode sizes were determined.

*Die nachstehende Arbeit wurde im Rahmen des Vertrages zwischen dem Institut für Plasmaphysik GmbH und der Europäischen Atomgemeinschaft über die Zusammenarbeit auf dem Gebiete der Plasmaphysik durchgeführt.*

TABLE OF CONTENTS

ABSTRACT

IPP 3/26     Z.N. Celinski     Two-Dimensional Analysis of MHD  
              F.W. Fischer     Generators with Segmented Elec-  
                                      trodes, January, 1965 (in English).

List of Symbols

1. INTRODUCTION

2. ABSTRACT:

The distribution of electrical parameters in MHD generators was determined by numerical analysis for any channel geometry and any practical Hall parameter. The analysis was limited to generators with a separate electrical circuit for each pair of electrodes. Constant gas dynamic parameters and constant generator cross-section were assumed. A correction factor  $\lambda$  was calculated, the use of which makes it possible to correct one-dimensional theory equations for two-dimensional effects. Optimum electrode sizes were determined.

3. RESUME

5.1 Generator Internal Resistance

5.1.1 General

5.1.2 Method for Determination of  $\lambda$

5.1.3 Results: Values of  $\lambda$

5.1.4 Empirical Formula for  $\lambda$

5.1.5 Optimum Electrode Size

5.2 Distribution of Electrical Parameters in MHD Channel

5.3 Current Distribution Along Electrode

5.4 Potential Distribution Along Insulator

5.5 Potential Distribution Between Opposite Electrodes

5.6 Current Density Distribution Along Channel Wall

5.7 Ohmic Loss Distribution

6. COMPARISON WITH OTHER WORK

6.1 Harwitz, Kilo, and Sutton

6.2 Schultz-Grunow and Denzel

6.3 Crown

TABLE OF CONTENTS

ABSTRACT

Table of Contents

List of Figures and Tables

List of Symbols

1. INTRODUCTION

2. SUMMARY

3. ASSUMPTIONS

4. THEORETICAL DEVELOPMENT

4.1 Basic Equations

4.2 Boundary Conditions

4.3 Properties of  $\gamma$ -Field

4.4 Potential Distribution

4.5 Other Properties of  $\varphi^*$ -Field

5. RESULTS AND DISCUSSION

5.1 Generator Internal Resistance

5.1.1 General

5.1.2 Method for Determination of  $\lambda$

5.1.3 Results: Values of  $\lambda$

5.1.4 Empirical Formula for  $\lambda$

5.1.5 Optimum Electrode Size

5.2 Distribution of Electrical Parameters in MHD Channel

5.3 Current Distribution Along Electrode

5.4 Potential Distribution Along Insulator

5.5 Potential Distribution Between Opposite Electrodes

5.6 Current Density Distribution Along Channel Wall

5.7 Ohmic Loss Distribution

6. COMPARISON WITH OTHER WORK

6.1 Hurwitz, Kilb, and Sutton

6.2 Schultz-Grunow and Denzel

6.3 Crown

LIST OF FIGURES

7. CONCLUSIONS

A. Appendix - Computer Programming

A.1 Field Description

A.2 Laplace Equation

A.3 Boundary Conditions

A.4 Programming for  $\gamma$  -Values

A.5 Programming for  $\varphi^*$  -Values

A.6 Programming for  $j$  -Values

A.7 Programming for Ohmic Losses

References and Acknowledgment

1. Dependence of  $\lambda$  on  $\beta$  and  $a/b$  for  $c/s = 0.2$
2. Dependence of  $\lambda$  on  $\beta$  and  $a/b$  for  $c/s = 0.4$
3. Dependence of  $\lambda$  on  $\beta$  and  $a/b$  for  $c/s = 0.6$
4. Dependence of  $\lambda$  on  $\beta$  and  $a/b$  for  $c/s = 0.8$
5. Range of Applicability of Empirical Formula for  $\lambda$
6. Values of  $D$  in Empirical Formula
7. Dependence of  $\lambda$  on  $c/s$
8. Optimum Electrode Width
9. Distribution of  $\gamma$  and  $\varphi^*$  for  $s/h = 2$ ,  $c/s = 0.25$ ,  $\beta = 0$
10. Distribution of  $\gamma$  and  $\varphi^*$  for  $s/h = 2$ ,  $c/s = 0.25$ ,  $\beta = 5$
11. Distribution of  $\gamma$  and  $\varphi^*$  for  $s/h = 2$ ,  $c/s = 0.75$ ,  $\beta = 0$
12. Distribution of  $\gamma$  and  $\varphi^*$  for  $s/h = 2$ ,  $c/s = 0.75$ ,  $\beta = 5$
13. Distribution of  $j_x$  and  $j_y$  for  $s/h = 2$ ,  $c/s = 0.25$ ,  $\beta = 0$
14. Distribution of  $j_x$  and  $j_y$  for  $s/h = 2$ ,  $c/s = 0.25$ ,  $\beta = 5$
15. Distribution of  $j_x$  and  $j_y$  for  $s/h = 2$ ,  $c/s = 0.75$ ,  $\beta = 0$
16. Distribution of  $j_x$  and  $j_y$  for  $s/h = 2$ ,  $c/s = 0.75$ ,  $\beta = 5$
17. Distribution of  $q$  for  $s/h = 2$ ,  $c/s = 0.25$ ,  $\beta = 0$
18. Distribution of  $q$  for  $s/h = 2$ ,  $c/s = 0.25$ ,  $\beta = 5$
19. Distribution of  $q$  for  $s/h = 2$ ,  $c/s = 0.75$ ,  $\beta = 0$
20. Distribution of  $q$  for  $s/h = 2$ ,  $c/s = 0.75$ ,  $\beta = 5$
21. Current Distribution Along Electrode for  $s/h = 0.15$ ,  $c/s = 0.83$  and  $s/h = 4$ ,  $c/s = 0.25$
22. Current Distribution Along Electrode for  $c/s = 0.25$  to  $0.83$

LIST OF FIGURES

1. Coordinate System
2. Field Distribution of  $\gamma$
3. Nomenclature for Potential Distribution
4. Current Distribution in an Ideal and in a Real Generator
5. Electrical Characteristics of Real and Ideal Generators
6. Dependence of  $\lambda$  on  $\beta$  and  $s/h$  for  $c/s = 0.2$
7. Dependence of  $\lambda$  on  $\beta$  and  $s/h$  for  $c/s = 0.4$
8. Dependence of  $\lambda$  on  $\beta$  and  $s/h$  for  $c/s = 0.6$
9. Dependence of  $\lambda$  on  $\beta$  and  $s/h$  for  $c/s = 0.8$
10. Range of Applicability of Empirical Formula for  $\lambda$
11. Values of D in Empirical Formula
12. Dependence of  $\lambda$  on  $c/s$
13. Optimum Electrode Width
14. Distribution of  $\gamma$  and  $\varphi^*$  for  $s/h = 2, c/s = 0.25, \beta = 0$
15. Distribution of  $\gamma$  and  $\varphi^*$  for  $s/h = 2, c/s = 0.25, \beta = 5$
16. Distribution of  $\gamma$  and  $\varphi^*$  for  $s/h = 2, c/s = 0.75, \beta = 0$
17. Distribution of  $\gamma$  and  $\varphi^*$  for  $s/h = 2, c/s = 0.75, \beta = 5$
18. Distribution of  $j_x$  and  $j_y$  for  $s/h = 2, c/s = 0.25, \beta = 0$
19. Distribution of  $j_x$  and  $j_y$  for  $s/h = 2, c/s = 0.25, \beta = 5$
20. Distribution of  $j_x$  and  $j_y$  for  $s/h = 2, c/s = 0.75, \beta = 0$
21. Distribution of  $j_x$  and  $j_y$  for  $s/h = 2, c/s = 0.75, \beta = 5$
22. Distribution of  $q$  for  $s/h = 2, c/s = 0.25, \beta = 0$
23. Distribution of  $q$  for  $s/h = 2, c/s = 0.25, \beta = 5$
24. Distribution of  $q$  for  $s/h = 2, c/s = 0.75, \beta = 0$
25. Distribution of  $q$  for  $s/h = 2, c/s = 0.75, \beta = 5$
26. Current Distribution Along Electrode for  $s/h = 0.15, c/s = 0.83$   
and  $s/h = 4, c/s = 0.25$
27. Current Distribution Along Electrode for  $c/s = 0.25$  to  $0.83$

- 28.  $\varphi^*$  Along Electrode and Insulator Wall
- 29.  $\varphi_y^*/\Delta\varphi_y^*$  Between Centers of Opposite Electrodes for  $s/h = 4$ ,  $c/s = 0.06$
- 30.  $\varphi_y^*/\Delta\varphi_y^*$  Between Centers of Opposite Electrodes for  $s/h = 0.15$ ,  $c/s = 0.17$
- 31.  $\varphi_y^*/\Delta\varphi_y^*$  Between Centers of Opposite Electrodes for  $s/h = 0.15$ ,  $c/s$  from 0.17 to 0.83
- 32.  $j_x$  and  $j_y$  Along Electrode and Insulator Wall for  $s/h = 2$ ,  $c/s = 0.25$
- 33.  $j_x$  and  $j_y$  Along Electrode and Insulator Wall for  $s/h = 2$ ,  $c/s = 0.75$
- 34. Total  $q$  Across Channel for  $s/h = 2$  and  $c/s = 0.25$  and 0.75
- 35.  $q$  Along Electrode and Insulator Wall for  $s/h = 2$ ,  $c/s = 0.25$
- 36.  $q$  Along Electrode and Insulator Wall for  $s/h = 2$ ,  $c/s = 0.75$
- 37.  $j_x/j_y$  at Center of Section for  $c/s = 0.5$  and 0.125
- 38.  $\lambda$  for  $c/s = 0.5$ , Comparison with Ref. [2]
- 39.  $R_p/R_{p.0}$  for  $s/h = 1.0$ , Comparison with Ref. [4]
- A.1  $1/\lambda$  for  $s/h = 0.5$ , Comparison with Ref. [3]
- A.2 Channel Schematic
- A.3 Schematic of Boundary Conditions for Computer Analysis
- A.4  $\gamma$  Along Electrodes for  $c/\Delta x = 32$ , Comparison with Ref. [3]
- A.5  $\gamma$  Along Electrodes for  $c/\Delta x = 10$ , Comparison with Ref. [3]

LIST OF TABLES

- I. Equations for Electrical Parameters (Two-Dimensional Theory)
  - A I. Electrode Boundary Equations

LIST OF SYMBOLS

$C$	Conductor Width
$h$	Electrode Separation
$\vec{j}$	Current Density Vector
$m, n$	Mesh Indices
$P$	Electrical Power Density
$P_m$	Brake Power Density
$q$	Ohmic Loss Density
$S$	Section Length
$\vec{w}$	Gas Velocity Vector
$x, y, z$	Coordinates
$A$	Constant in Eq. (91)
$\vec{B}$	Magnetic Induction Vector
$D$	Constant in Eq. (91)
$\vec{E}$	Electrical Field Vector in Laboratory System
$\vec{E}^*$	Electrical Field Vector in System Moving with Fluid
$H$	Electrode Separation
$J$	Total Current
$K$	Load Factor
$P$	Electrical Power
$P_m$	Brake Power
$Q$	Ohmic Losses
$R$	Generator Internal Resistance
$R_a$	External Resistance
$S$	Normalized Section Length
$T$	Width of Generator Channel
$U$	Terminal Voltage



$\beta$	Electron Hall Parameter
$\chi$	Current Flux Function
$\eta$	Electrical Efficiency
$\theta$	Angle Between $\vec{j}$ and $\vec{E}^*$
$\lambda$	Correction Factor
$\sigma$	Electrical Conductivity
$\sigma_{\text{eff}}$	Effective Electrical Conductivity
$\sigma_0$	Electrical Conductivity with $\vec{B} = 0$
$\varphi^*$	Electrical Potential
$\Delta x, \Delta y$	Dimension of Area Element

SUBSCRIPTS

$a$	(See $R_a$ above)
$i$	Ideal Generator ( $s/h = 0$ )
$K$	Short Circuit
$m$	(See $P_m$ above)
$o$	$\vec{B} = 0$ or Open Circuit

WORKING et al. [1], BRUN [2], and SCHWILZ-GRUNOW & DENZEL [3] investigated the behavior of finite-length electrodes on electrical parameters. In [1] and [2] best efforts to solve the problem analytically, but analytical solutions are presented upon the introduction of simplifying assumptions which results are not sufficiently general. Reference [3] describes a method for numerical solution, limited to small values of  $\beta$ . In the present report, an improved numerical analysis is developed to include also solutions for large values of  $\beta$ .

## 1. INTRODUCTION

The one-dimensional theory of MHD generators with segmented electrodes [1] is based upon the assumption that the electrical field and the current density are homogeneous in the generator channel. This is equivalent to assuming the ideal case of infinitely segmented electrodes.

In a real generator, the electrodes have finite dimensions, and two-dimensional analysis must be applied. Electrode end-effects appear, influencing the electrical parameters of the generator even when  $\beta = \omega\tau \approx 0$ . With increasing  $\beta$ , the Hall potential increases. The Hall field near finite-length electrodes is shorted (electrodes forming equipotential surfaces), causing current concentration on one edge of the electrode. The result is an increase in the internal resistance and thus a deterioration of the efficiency of the generator. This effect is a function of channel geometry and magnitude of the Hall parameter  $\beta$ .

The purpose of the work reported here is: first, the determination of the deviation of all electrical parameters from their theoretical one-dimensional theory values, and second, the quantitative investigation of the distribution of electrical parameters, including ohmic losses. Numerical analysis was employed. An IBM 7090 computer was used.

HURWITZ et al [2], CROWN [3], and SCHULTZ-GRUNOW & DENZEL [4] investigated the influence of finite-length electrodes on electrical parameters. References [2] and [4] were efforts to solve the problem analytically; but analytical solutions are predicated upon the introduction of simplifying assumptions which usually are not sufficiently general. Reference [3] describes a method for numerical solution, limited to small values of  $\beta$ . In the present report, an improved numerical analysis is developed to include also solutions for large values of  $\beta$ .

## 2. SUMMARY

The distributions of electrical parameters in an MHD generator were determined for any generator geometry and any Hall parameter. The analysis was limited to generators with a separate electrical circuit for each pair of electrodes. Numerical analysis was used and calculations were made on an IBM 7090.

From this distribution a correction factor  $\lambda$  was calculated, the use of which makes it possible to correct one-dimensional theory equations for two-dimensional effects.

This analysis was made assuming constant gas dynamical parameters and constant channel cross-section.

The influence of finite size electrodes on electrical parameters in MHD generators is generally large. Optimum electrode sizes were determined.

Ohmic losses have a steep gradient across the channel, and, therefore, the distribution of these losses must be taken into account when considering electron heating.

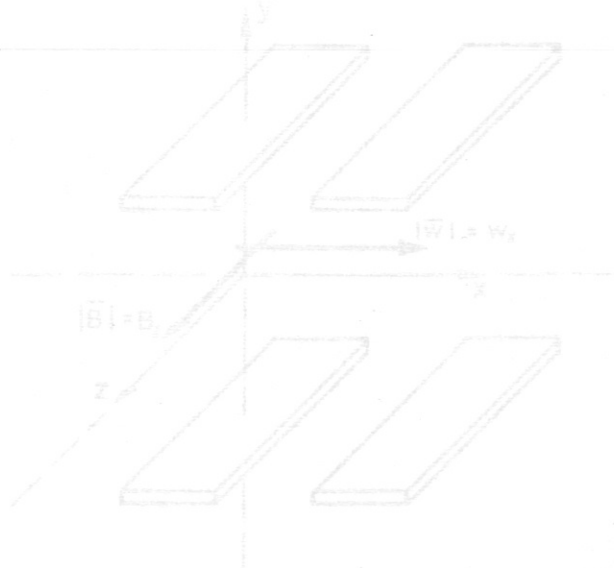


Fig. 1. Coordinate System

### 3. ASSUMPTIONS

The following assumptions were made:

- a. Gas dynamic parameters are constant ( $\rho, T, w = \text{constant}$ ).  
 $\bar{w} = (w_x, 0, 0)$ .  
 $\sigma_0$  is constant (thermal equilibrium between electrons and atoms is also assumed).
- b. Channel cross-section is constant.
- c. Applied magnetic field  $\bar{B}$  is constant.  $\bar{B} = (0, 0, B_z)$ .  
Induced magnetic field is ignored (magnetic Reynold's number  $\ll 1$ ).
- d. Channel endeffects are excluded.
- e. Electrode effects other than Hall field shorting are ignored.
- f. Ion slip is ignored.
- g. Figure 1 shows the coordinate system.

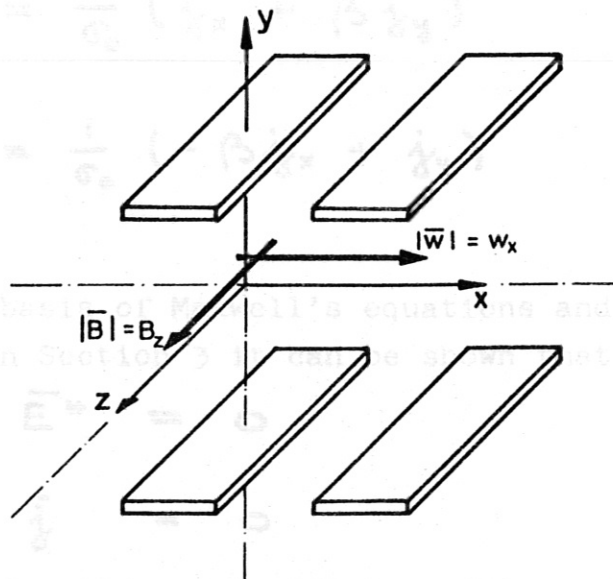


Fig. 1 Coordinate System

#### 4. THEORETICAL DEVELOPMENT

##### 4.1 Basic Equations

Ohm's law may be written as

$$\bar{j} = \sigma_0 \bar{E}^* - \frac{\beta}{B} [\bar{j} \times \bar{B}] \quad (1)$$

where

$$\bar{E}^* = \bar{E} + [\bar{\omega} \times \bar{B}] \quad (2)$$

Equation (1) may be developed in two components

$$j_x = \frac{\sigma_0}{1 + \beta^2} (E_x^* - \beta E_y^*) \quad (3)$$

$$j_y = \frac{\sigma_0}{1 + \beta^2} (\beta E_x^* + E_y^*) \quad (4)$$

or

$$E_x^* = \frac{1}{\sigma_0} (j_x + \beta j_y) \quad (5)$$

$$E_y^* = \frac{1}{\sigma_0} (-\beta j_x + j_y) \quad (6)$$

On the basis of Maxwell's equations and the assumptions in Section 3 it can be shown that

$$\nabla \times \bar{E}^* = 0 \quad (7)$$

$$\nabla \cdot \bar{j} = 0 \quad (8)$$

Use of Equations (5), (6), and (7) results in

$$\frac{\partial j_x}{\partial x} - \beta \frac{\partial j_x}{\partial x} - \beta \frac{\partial j_x}{\partial y} - \frac{\partial j_x}{\partial y} = 0 \quad (9)$$

Using (8),

$$\frac{\partial j_y}{\partial x} - \frac{\partial j_x}{\partial y} = 0 \quad (10)$$

The current flux function is defined as

$$j_x = \frac{\partial \gamma}{\partial y} \quad (11)$$

$$j_y = - \frac{\partial \gamma}{\partial x} \quad (12)$$

Substitution of Equations (11) and (12) into (10) yields

$$\frac{\partial^2 \gamma}{\partial x^2} + \frac{\partial^2 \gamma}{\partial y^2} = 0 \quad (13)$$

The current flux function  $\gamma$  as defined in (11) and (12) satisfies the Laplace Equation (13). Equation (13) forms the basis of the numerical analysis. The mathematical solution of the Laplace equation for specific boundary conditions is shown in the Appendix.

#### 4.2 Boundary Conditions

##### 4.2.1 On the electrode surface

$$E_x = 0 \quad (14)$$

where

$$|E_x| = |E_x^*| \quad (15)$$

Therefore, from (5), (11), and (12)

$$- \frac{j_x}{j_y} = \frac{\partial \gamma / \partial y}{\partial \gamma / \partial x} = \beta \quad (16)$$

4.2.2 On the insulator surface

$$j_y = 0 \tag{17}$$

and with (12)

$$\gamma = \text{constant} \tag{18}$$

### 4.3 Properties of the $\gamma$ -Field

4.3.1 The  $\gamma$  distribution is repeated in each section of the generator. Therefore, the analysis can be limited to one section (see Fig. 2).

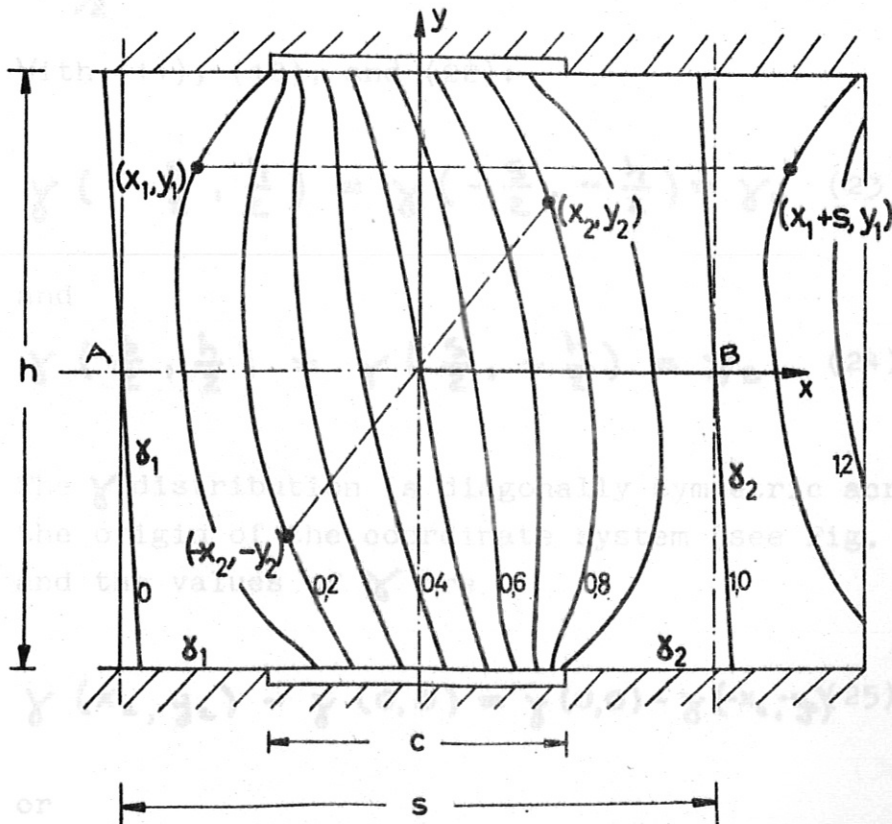


Fig. 2 Field Distribution of  $\gamma$

From symmetry and periodicity of section

$$\gamma(x_1, y_1) + \Delta\gamma = \gamma(x_1 + s, y_1) \quad (19)$$

$$\Delta\gamma = \gamma_2 - \gamma_1 \quad (20)$$

where  $\gamma = \gamma_1$  passes through point **A** and  
 $\gamma = \gamma_2$  passes through point **B** in Fig. 2.

4.3.2 Since the entire current must flow from one electrode to the opposite electrode:

$$\int_{-h/2}^{+h/2} j_x(-\frac{s}{2}, y) dy = 0 \quad (21)$$

and

$$\int_{-h/2}^{+h/2} j_x(\frac{s}{2}, y) dy = 0 \quad (22)$$

With (11), (12), and (22):

$$\gamma(-\frac{s}{2}, \frac{h}{2}) = \gamma(-\frac{s}{2}, -\frac{h}{2}) = \gamma_1 \quad (23)$$

and

$$\gamma(\frac{s}{2}, \frac{h}{2}) = \gamma(\frac{s}{2}, -\frac{h}{2}) = \gamma_2 \quad (24)$$

4.3.3 The  $\gamma$  distribution is diagonally symmetric across the origin of the coordinate system (see Fig. 2), and the values of  $\gamma$  are.

Then

$$\gamma(x_2, y_2) - \gamma(0,0) = \gamma(0,0) - \gamma(-x_2, -y_2) \quad (25)$$

or

$$\gamma(x_2, y_2) + \gamma(-x_2, -y_2) = 2\gamma(0,0) = \gamma_1 + \gamma_2 \quad (26)$$



From symmetry and periodicity of section

$$\gamma\left(-\frac{s}{2}, y\right) + \gamma\left(-\frac{s}{2}, -y\right) = 2\gamma_1 \quad (27)$$

$$\gamma\left(+\frac{s}{2}, y\right) + \gamma\left(+\frac{s}{2}, -y\right) = 2\gamma_2 \quad (28)$$

Also,  $\gamma\left(-\frac{s}{2}, 0\right) = \gamma_1 \quad (29)$

$$\gamma\left(+\frac{s}{2}, 0\right) = \gamma_2 \quad (30)$$

4.3.5 From boundary condition on electrode, Section 4.2.1,

$$-\frac{j_x}{j_y} = \beta \quad (31)$$

i.e., the flux lines enter the electrodes always at the same angle with the normal to the surface

$$\theta = \tan^{-1} \beta \quad (32)$$

#### 4.4 Potential Distribution

Since  $\nabla \times \bar{E}^* = 0$  (see Eq. (7))

we can define a potential function  $\varphi^*$  (36)

$$\sigma_0 \bar{E}^* = -\nabla \varphi^* \quad (33)$$

Then

$$\sigma_0 E_y^* = -\partial \varphi^* / \partial y \quad (34)$$

Taking point  $(x_1, y_1)$  at the center of the lower electrode and  $(x_1, y_1)$  at the center of the upper electrode  $(x_1, y_1 = h/2)$ , Equation (35) becomes

$$\varphi^*(x, y) = \varphi^*(x_1, y_1) + \beta [\gamma(x, y) - \gamma(x_1, y_1)] + \int_{y_1}^y \frac{\partial}{\partial x} \gamma(x, y) dy \quad (35)$$

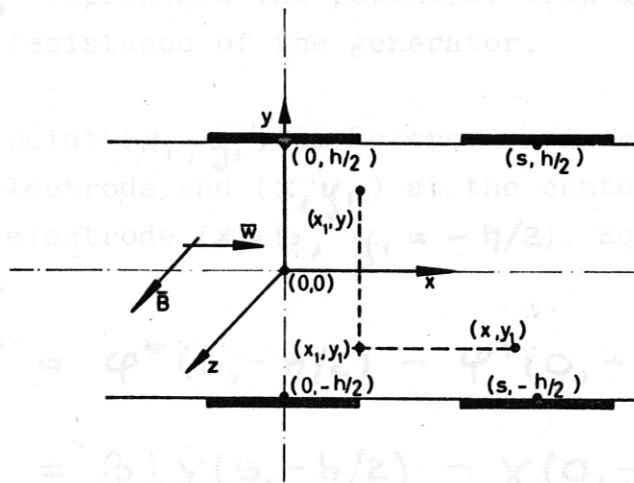


Fig. 3 Nomenclature for Potential Distribution

$\Delta\varphi^*/\sigma_0$  represents the potential difference between the electrodes. From (33) also

$$\sigma_0 E_x^* = - \frac{\partial \varphi^*}{\partial x} \quad (36)$$

with (5), (11), and (12) the angle between vectors  $\mathbf{j}$  and  $\mathbf{E}^*$  is equal to

$$\varphi^*(x, y_1) = \varphi^*(x_1, y_1) + \beta [\gamma(x, y_1) - \gamma(x_1, y_1)] - \int_{x_1}^x \frac{\partial}{\partial y} \gamma(x, y_1) dx \quad (37)$$

Taking point  $(x_1, y_1)$  at the center of the lower electrode ( $x_1 = 0, y_1 = -h/2$ ) and  $(x_1, y_1)$  at the center of the upper electrode ( $x_1 = 0, y_1 = h/2$ ), Equation (35) becomes

$$\begin{aligned} \Delta \varphi_y^* &= \varphi^*(0, h/2) - \varphi^*(0, -h/2) \\ &= \beta [\gamma(0, h/2) - \gamma(0, -h/2)] \\ &\quad + \int_{-h/2}^{+h/2} \frac{\partial}{\partial x} \gamma(0, y) dy \end{aligned} \quad (38)$$

$\Delta \varphi_y^* / \sigma_0$  represents the potential drop across the internal resistance of the generator.

Taking point  $(x_1, y_1)$  as before at the center of the lower electrode and  $(x, y_1)$  at the center of the neighboring electrode ( $x = s, y_1 = -h/2$ ), Equation (37) becomes

$$\begin{aligned} \Delta \varphi_x^* &= \varphi^*(s, -h/2) - \varphi^*(0, -h/2) \\ &= \beta [\gamma(s, -h/2) - \gamma(0, -h/2)] \\ &\quad - \int_0^s \frac{\partial}{\partial y} \gamma(x, -h/2) dx \end{aligned} \quad (39)$$

$\Delta \varphi_x^* / \sigma_0$  represents the potential difference between two neighboring electrodes.

#### 4.5 Other Properties of the $\varphi^*$ -Field

4.5.1 From Equation (1), the angle between vectors  $\vec{j}$  and  $\vec{E}^*$  is equal to

$$\theta = \tan^{-1} \beta \quad (40)$$

Since  $\vec{j}$  is tangential to lines of constant  $\gamma$ , and since  $\vec{E}^*$  is normal to lines of constant  $\varphi^*$ , the angle between  $\gamma = \text{constant}$  and  $\varphi^* = \text{constant}$

4. RESULTS AND DISCUSSION

Taking  $\psi = 0$  and  $\psi = \beta$ , the Laplace Equation (13) was solved and is equal to

$$\theta' = 90^\circ - \theta = \text{ctn}^{-1} \beta \quad (41)$$

4.5.2 From insulator boundary conditions, Section 4.2.2 and Equation (4)

$$-\frac{E_y^*}{E_x^*} = \beta \quad (42)$$

i.e., the vector  $\vec{E}^*$  always meets the insulator surface at the same angle  $\tan^{-1} \beta$ . Lines of constant  $\psi^*$  meet the insulator at an angle

$$\theta' = \text{ctn}^{-1} \beta \quad (43)$$

4.1.1 General

In-homogeneous current distribution in the channel due to finite size of the electrodes increases the internal resistance of the generator. This, in turn, causes a reduction in terminal voltage, current, electrical power, and electrical efficiency, and also an increase in ohmic losses.

A dimensionless parameter  $\lambda$  is defined as

$$\lambda = \frac{R_i}{R} = \frac{h}{s} \frac{\int_{\psi_1}^{\psi_2} i_1 dx}{\int_{\psi_1}^{\psi_2} i dx} \leq 1 \quad (44)$$

where  $\ell$  is measured along any  $\psi = \text{constant}$  line.

5. RESULTS AND DISCUSSION

Taking  $\gamma_1 = 0$  and  $\gamma_2 = 1$ , the Laplace Equation (13) was solved numerically by an iteration method on the IBM 7090. See Appendix.

The analysis was made for three variable parameters: two geometric:  $s/h$  and  $c/s$ , and Hall parameter  $\beta$ . The following ranges were used:

$$\begin{aligned}
 0.15 &\leq \frac{s}{h} \leq 4 \\
 0.06 &< \frac{c}{s} < 0.875 \\
 0 &\leq \beta \leq 10
 \end{aligned}$$

Taking  $\varphi^* = 0$  on the lower electrode, the  $\varphi^*$ - field was calculated from (35) and (37).

Current density and ohmic loss distributions were calculated on the basis of (11) and (12).

All results are normalized to values for an ideal MHD generator ( $s/h = 0$ ).

Fig. 4 Current distribution in an ideal and in a real generator

5.1 Generator Internal Resistance

5.1.1 General

Inhomogeneous current distribution in the channel due to finite size of the electrodes increases the internal resistance of the generator. This, in turn, causes a reduction in terminal voltage, current, electrical power, and electrical efficiency, and also an increase in ohmic losses.

A dimensionless parameter  $\lambda$  is defined as

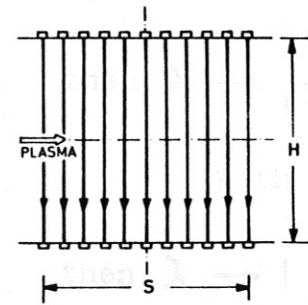
$$\lambda = \frac{R_i}{R} = \frac{h}{s} \frac{\int_{-s/2}^{+s/2} j_y dx}{\int_0^l j dl} \leq 1 \tag{44}$$

where  $l$  is measured along any  $\gamma = \text{constant}$  line.

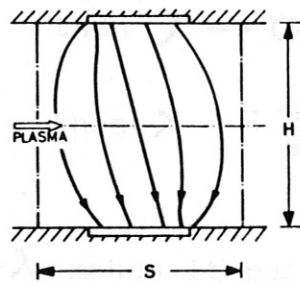
Equation (47) defines  $\sigma_{\text{eff}}$

Parameter  $\lambda$  is a function of  $\nu, h$  and  $e$ , and  $\rho$ .

Special cases are



IDEAL GENERATOR



REAL GENERATOR

Fig. 4 Current Distribution in an ideal and in a real generator

$\lambda$  is a measure of the increase of the internal resistance  $R$  of a real generator over the internal resistance  $R_i$  of an ideal generator (Fig. 4) for the same generator volume element  $H \times s \times T$

Since

$$R_i = \frac{1}{\sigma_0} \frac{H}{sT} \quad (45)$$

and

$$R = \frac{1}{\sigma_{eff}} \frac{H}{sT} \quad (46)$$

it follows that

$$\lambda = \frac{\sigma_{eff}}{\sigma_0} \quad (47)$$

Equation (47) defines  $\sigma_{eff}$ .

Parameter  $\lambda$  is a function of  $s, h$  and  $c$ , and  $\beta$ .

Special cases are:

if  $\frac{c}{s} \rightarrow 1$ , then  $\lambda \rightarrow \frac{1}{1+\beta^2}$  (generator with continuous electrodes)

if  $\frac{s}{h} \rightarrow 0$ , then  $\lambda \rightarrow 1$  (infinitely segmented electrodes)

if  $\frac{c}{s} \rightarrow 0$ , then  $\lambda \rightarrow 0$

if  $\frac{s}{h} \rightarrow \infty$ , then  $\lambda \rightarrow \frac{c}{s} \frac{1}{1+\beta^2}$

The introduction of  $\lambda$  makes it possible to determine, in a simple fashion, all electrical parameters of a real generator. In Table I, the equations for electrical parameters of ideal and of real generators are compared.

Relative values of electrical parameters were calculated with the use of Table I. It was assumed that  $R_a$ ,  $\sigma_0$ ,  $B$  and gasdynamic parameters are the same in the real and in the ideal generator. Equation (82) lists these relative values.

$$\begin{aligned} \left(\frac{K}{K_i}\right)_* &= \frac{j_y}{j_{yi}} = \left(\frac{E_y}{E_{yi}}\right)_* = \left(\frac{p}{p_i}\right)_*^{1/2} \\ &= \left(\frac{U}{U_i}\right)_* = \frac{j}{j_i} = \left(\frac{P}{P_i}\right)_*^{1/2} = \left(\lambda \frac{Q}{Q_i}\right)_*^{1/2} \\ &= \frac{P_m}{P_{mi}} = \left(\frac{\eta}{\eta_i}\right)_* = \boxed{\frac{R_a + R_i}{R_a + R_i/\lambda}} \quad (82) \end{aligned}$$

where  $( )_*$  means that equality holds only for  $R_a > 0$ . In all other cases, for short-circuit ( $R_a = 0$ ), the right side of (82) is equal to  $\lambda$ . For open-circuit ( $R_a = \infty$ ), the right side of (82) is equal to 1.

IDEAL GENERATOR ( $s/h = 0$ )	REAL GENERATOR ( $s/h > 0$ )
$K_i = R_a / (R_a + R_i)$ (48)	$K = R_a / (R_a + R_i / \lambda)$ (49)
$= U_i / U_{oi}$ (50)	$= U / U_o$ (51)
$= 1 - (J_i / J_{ki})$ (52)	$= 1 - (J / J_k)$ (53)
$E_{yi} = K_i w B$ (54)	$E_y = K w B$ (55)
$j_{yi} = (1 - K_i) \sigma_o w B$ (56)	$j_y = (1 - K) \lambda \sigma_o w B$ (57)
$p_i = K_i (1 - K_i) \sigma_o w^2 B^2$ (58)	$p = K (1 - K) \lambda \sigma_o w^2 B^2$ (59)
$U_i = K_i w B H$ (60)	$U = K w B H$ (61)
$= R_a w B H / (R_a + R_i)$ (62)	$= R_a w B H / (R_a + R_i / \lambda)$ (63)
$J_i = (1 - K_i) \sigma_o w B S T$ (64)	$J = (1 - K) \lambda \sigma_o w B S T$ (65)
$= w B H / (R_a + R_i)$ (66)	$= w B H / (R_a + R_i / \lambda)$ (67)
$P_i = K_i (1 - K_i) \sigma_o w^2 B^2 H S T$ (68)	$P = K (1 - K) \lambda \sigma_o w^2 B^2 H S T$ (69)
$= R_a (w B H)^2 / (R_a + R_i)^2$ (70)	$= R_a (w B H)^2 / (R_a + R_i / \lambda)^2$ (71)
$Q_i = (1 - K_i)^2 \sigma_o w^2 B^2 H S T$ (72)	$Q = (1 - K)^2 \lambda \sigma_o w^2 B^2 H S T$ (73)
$= R_i (w B H)^2 / (R_a + R_i)^2$ (74)	$= (R_i / \lambda) (w B H)^2 / (R_a + R_i / \lambda)^2$ (75)
$P_m = P_i + Q_i$ (76)	$P_m = P + Q$ (77)
$= (w B H)^2 / (R_a + R_i)$ (78)	$= (w B H)^2 / (R_a + R_i / \lambda)$ (79)
$\eta_i = P_i / P_m = K_i$ (80)	$\eta = P / P_m = K$ (81)

TABLE I EQUATIONS FOR ELECTRICAL PARAMETERS  
(TWO-DIMENSIONAL THEORY)



On the assumption of equal  $\sigma_0$ ,  $B$ , and gasdynamic parameters, but different  $R_a$ , the maximum electrical power occurs at  $K = K_i = 0.5$ , thus

$$P_{\text{MAX}} = \lambda P_{i\text{MAX}} \quad (83)$$

Fig. 5 shows the electrical characteristics for real and ideal generators, based on equations in Table I. All primed parameters in Fig. 5 are normalized and dimensionless:

$$U' = \frac{U}{wBH} \quad (84)$$

$$J' = \frac{J}{\sigma_0 wBST} \quad (85)$$

$$P' = \frac{P}{\sigma_0 w^2 B^2 HST}; \quad Q' = \frac{Q}{\sigma_0 w^2 B^2 HST};$$

$$P'_m = \frac{P_m}{\sigma_0 w^2 B^2 HST} \quad (86)$$

### 5.1.2 Method for Determination of $\lambda$

For the same total current with various geometries and  $B$ , the potential difference across the internal resistance,  $\Delta \varphi_y^* / \sigma_0$ , is determined from Equation (38).

The internal resistance of one section with one electrode pair is

$$R = \frac{\Delta \varphi_y^*}{\sigma_0} \frac{1}{J} \quad (87)$$

In an ideal generator, the internal resistance of a volume element of the same dimensions ( $h \times s \times T$ ) is

$$R_i = \frac{1}{\sigma_0} \frac{h}{sT} \quad (88)$$

Using (44), (87), and (88) results in

$$\lambda = \frac{1}{\alpha \beta} \frac{K}{K_i} \frac{3}{\beta} \quad (89)$$

In the quantitative analysis,  $\beta$  was set equal to 1, and  $\gamma = 1$  (two-dimensional analysis). Thus,

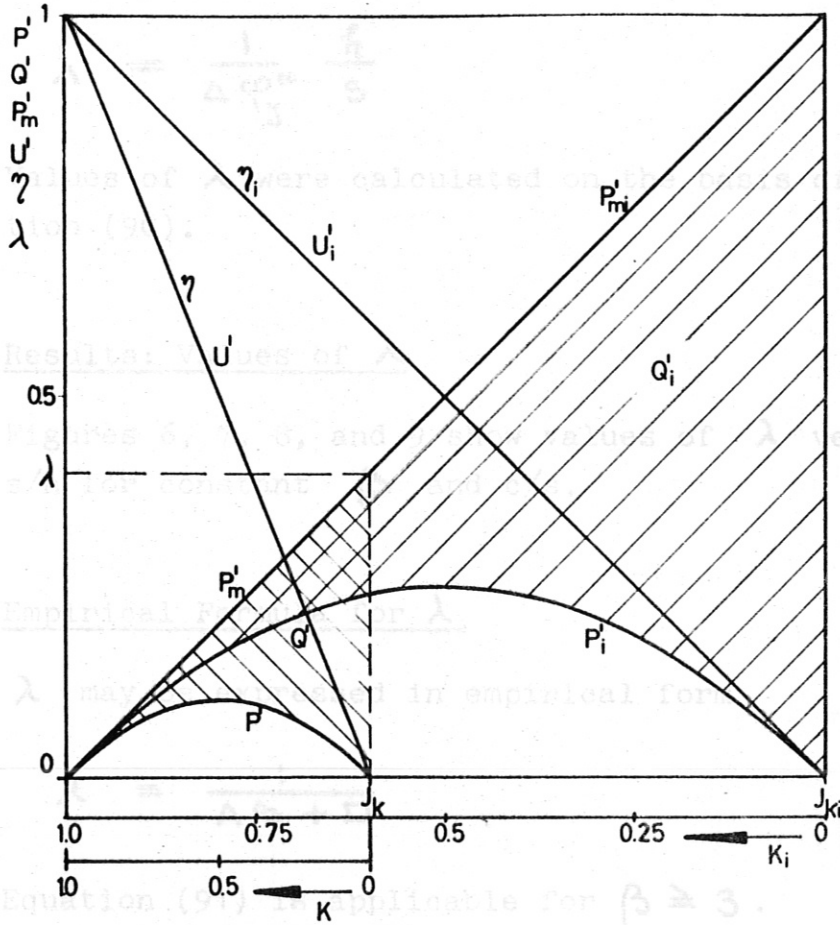


Fig.5 Electrical Characteristics of Real and Ideal generators

Using (44), (87), and (88) results in

$$\lambda = \frac{1}{\Delta \varphi_y^*} \frac{k}{s} \frac{J}{T} \quad (89)$$

In the quantitative analysis,  $J$  was set equal to 1, and  $T = 1$  (two-dimensional analysis). Thus,

$$\lambda = \frac{1}{\Delta \varphi_y^*} \frac{k}{s} \quad (90)$$

Values of  $\lambda$  were calculated on the basis of Equation (90).

### 5.1.3 Results: Values of $\lambda$

Figures 6, 7, 8, and 9 show values of  $\lambda$  versus  $s/h$  for constant  $\beta$  and  $c/s$ .

### 5.1.4 Empirical Formula for $\lambda$

$\lambda$  may be expressed in empirical form

$$\lambda = \frac{1}{A\beta + D} \quad (91)$$

Equation (91) is applicable for  $\beta \geq 3$ .

However, (91) may also be used for  $\beta \geq 2$  when  $s/h$  is small ( $s/h \leq 1$ ). See also Fig. 10. Equation (91) is more exact for larger  $\beta$ . Values of  $\lambda$  for  $\beta = 20$  were investigated and (91) was found to hold. The analysis was limited to  $s/h \leq 4$ .

For small  $s/h$ ,  $A$  is practically independent of  $c/s$ , and is equal to  $s/h$ . When  $s/h \leq 1$ , values of  $A$  differ from  $s/h$  by less than 1%; when  $s/h \leq 2$ , by less than 2%. For  $s/h = 4$ , the dependence of  $A$  on  $c/s$  becomes noticeable:

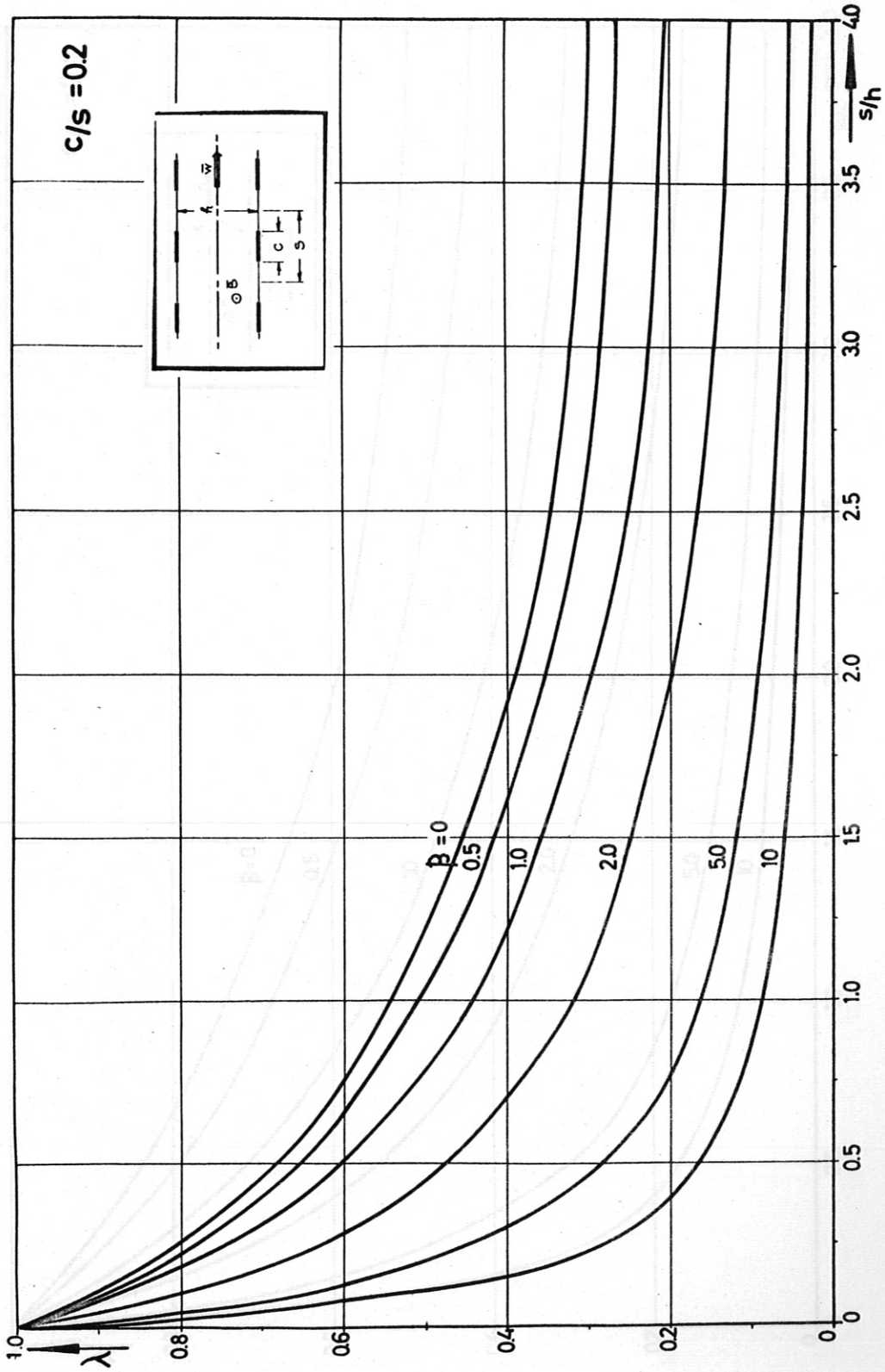


Fig. 6 Dependence of  $\lambda$  on  $\beta$  and  $s/h$  for  $c/s = 0.2$

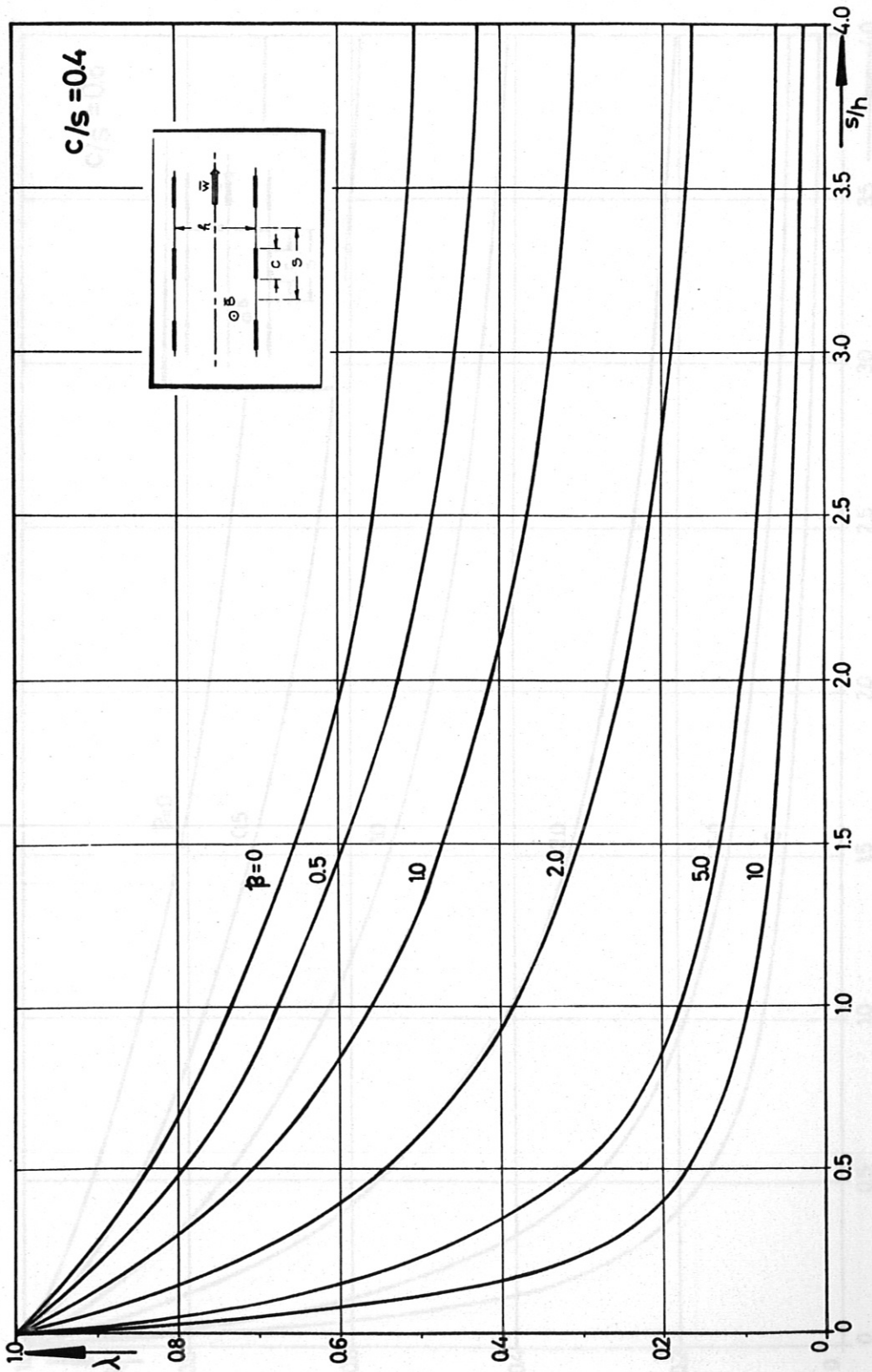


Fig. 7 Dependence of  $\lambda$  on  $\beta$  and  $s/h$  for  $c/s = 0.4$

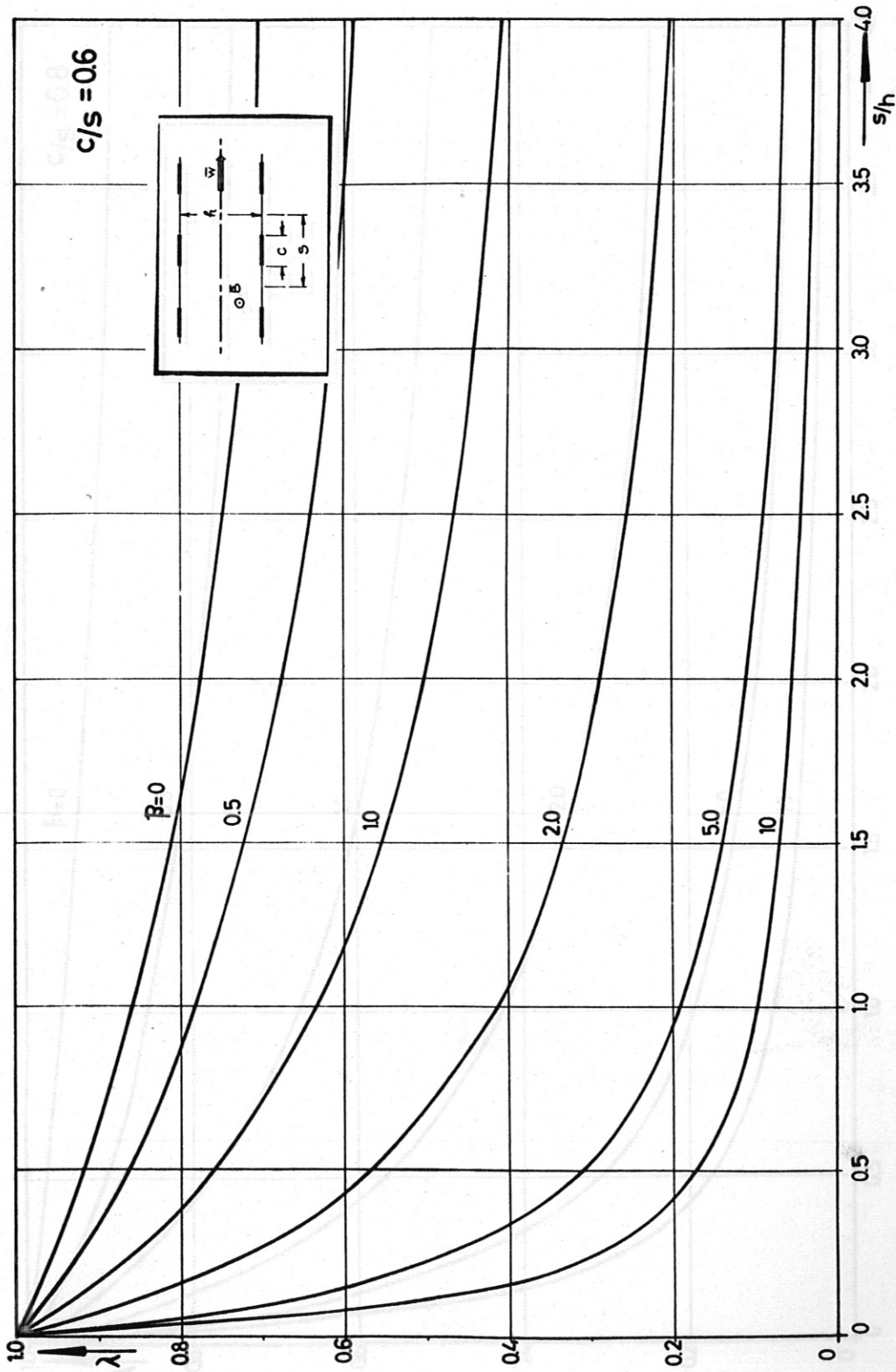


Fig. 8 Dependence of  $\lambda$  on  $\beta$  and  $s/h$  for  $c/s = 0.6$

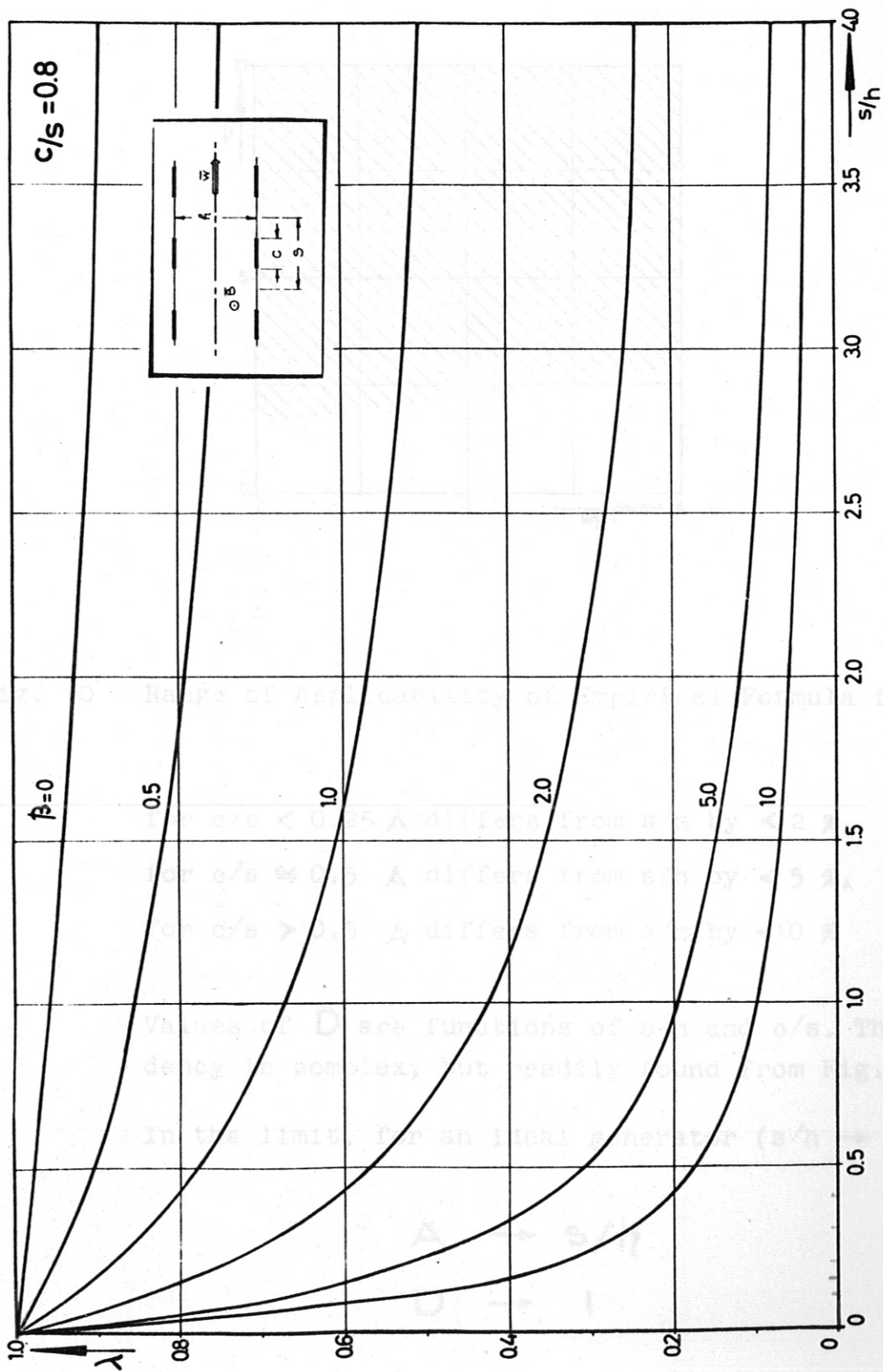


Fig. 9 Dependence of  $\lambda$  on  $\beta$  and  $s/h$  for  $c/s = 0.8$

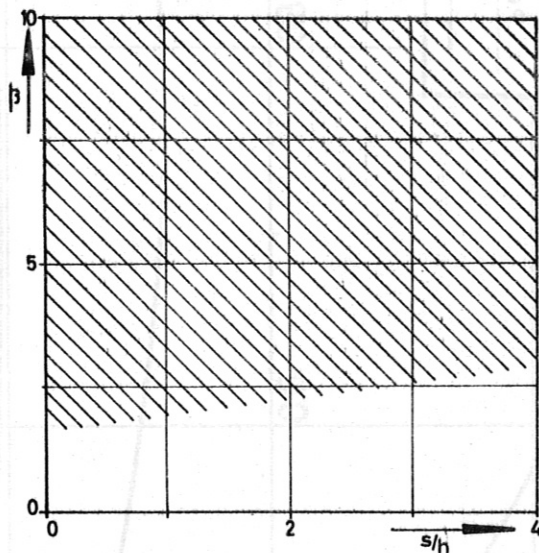


Fig. 10 Range of Applicability of Empirical Formula for  $\lambda$

for  $c/s < 0.25$   $\lambda$  differs from  $s/h$  by  $< 2\%$ ,  
 for  $c/s \approx 0.5$   $\lambda$  differs from  $s/h$  by  $< 5\%$ ,  
 for  $c/s > 0.5$   $\lambda$  differs from  $s/h$  by  $< 10\%$

Values of  $D$  are functions of  $s/h$  and  $c/s$ . This dependency is complex, but readily found from Fig. 11.

In the limit, for an ideal generator ( $s/h \rightarrow 0$ ),

$$\lambda \rightarrow s/h$$

$$D \rightarrow 1$$

and therefore,  $\lambda \rightarrow 1$ .

Fig. 11 Values of D in Empirical Formula



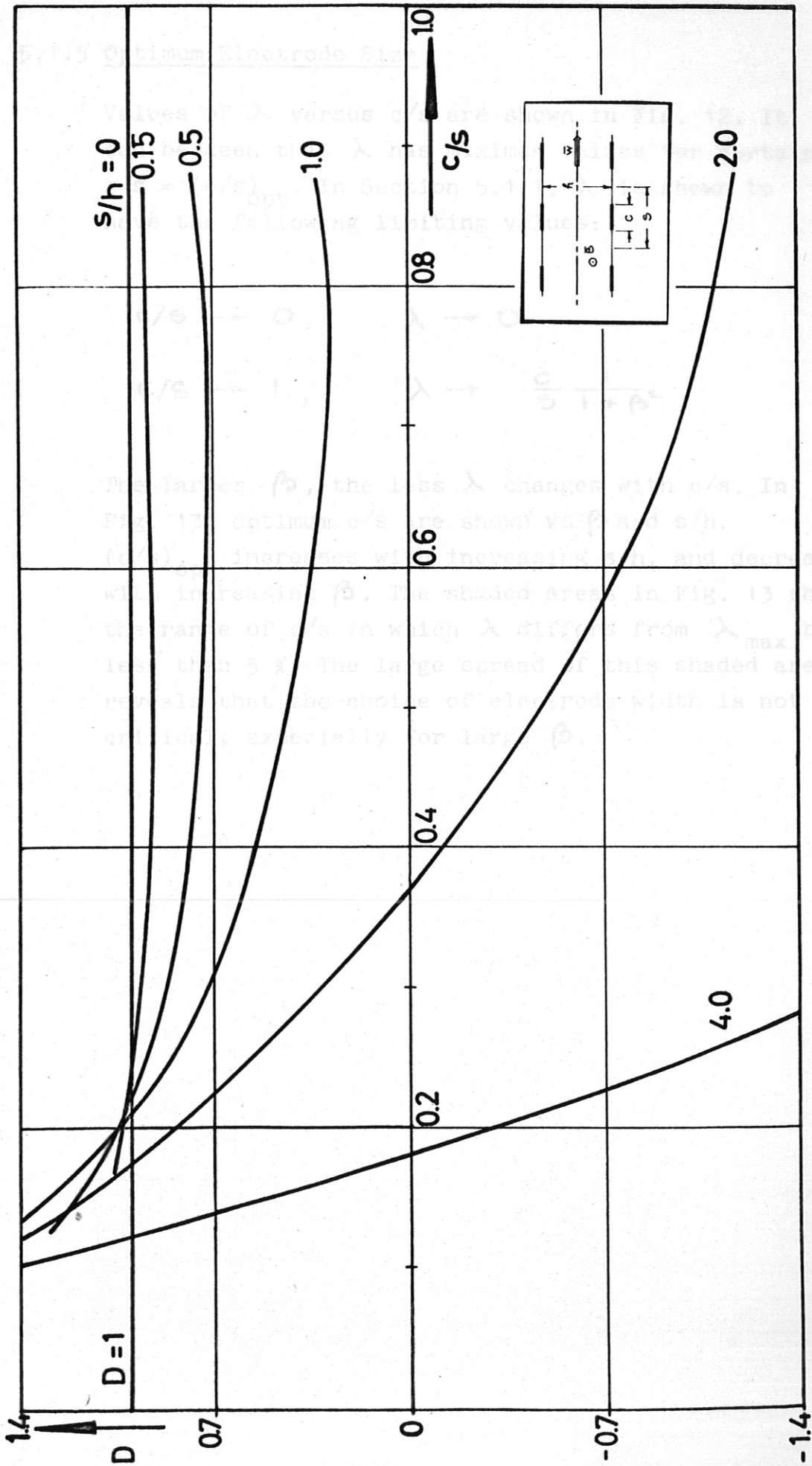


Fig. 11 Values of  $D$  in Empirical Formula

### 5.1.5 Optimum Electrode Size

Values of  $\lambda$  versus  $c/s$  are shown in Fig. 12. It can be seen that  $\lambda$  has maximum values for certain  $c/s = (c/s)_{opt}$ . In Section 5.1.1,  $\lambda$  is shown to have the following limiting values:

$$c/s \rightarrow 0, \quad \lambda \rightarrow 0$$

$$c/s \rightarrow 1, \quad \lambda \rightarrow \frac{c}{s} \frac{1}{1 + \beta^2}$$

The larger  $\beta$ , the less  $\lambda$  changes with  $c/s$ . In Fig. 13, optimum  $c/s$  are shown vs  $\beta$  and  $s/h$ .  $(c/s)_{opt}$  increases with increasing  $s/h$ , and decreases with increasing  $\beta$ . The shaded areas in Fig. 13 show the range of  $c/s$  in which  $\lambda$  differs from  $\lambda_{max}$  by less than 5%. The large spread of this shaded area reveals that the choice of electrode width is not critical, especially for large  $\beta$ .

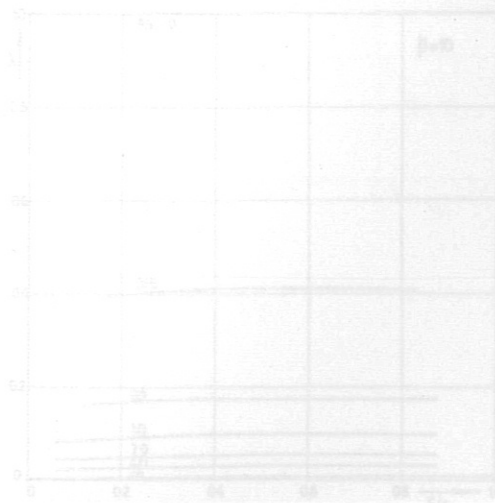
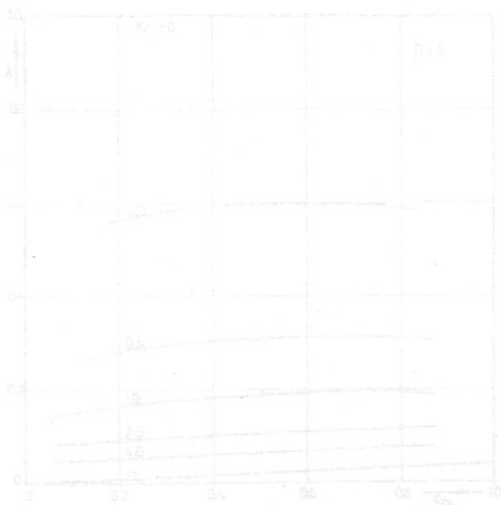
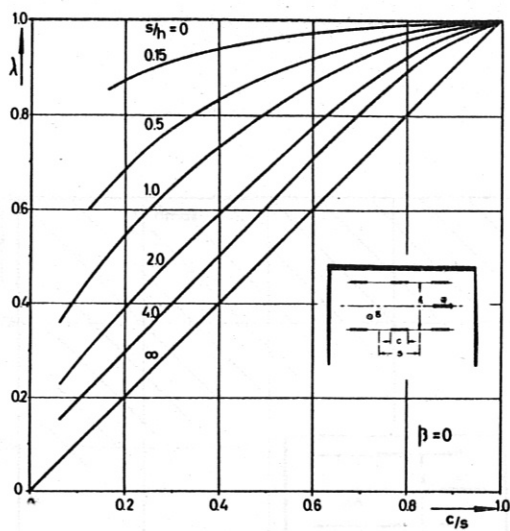
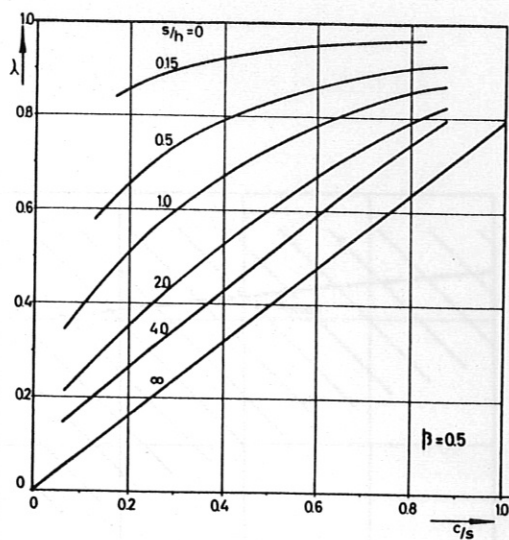


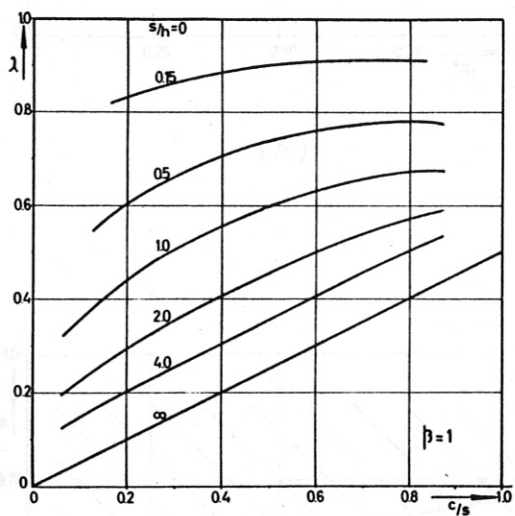
Fig. 12 Dependence of  $\lambda$  on  $c/s$



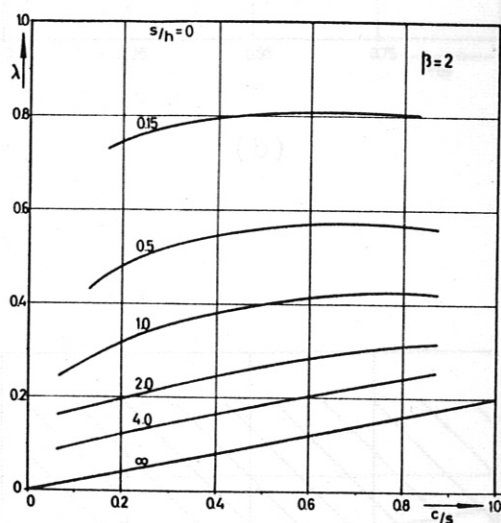
(a)



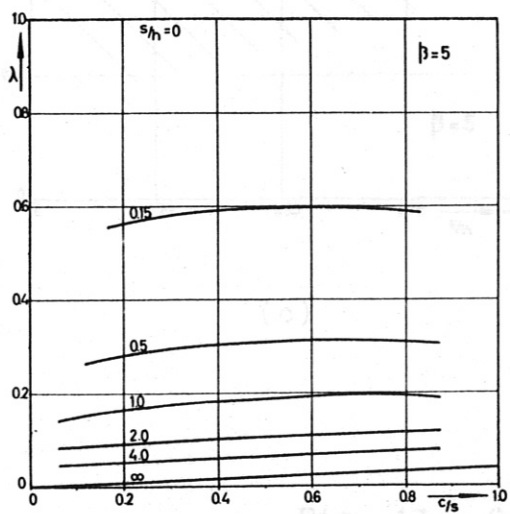
(b)



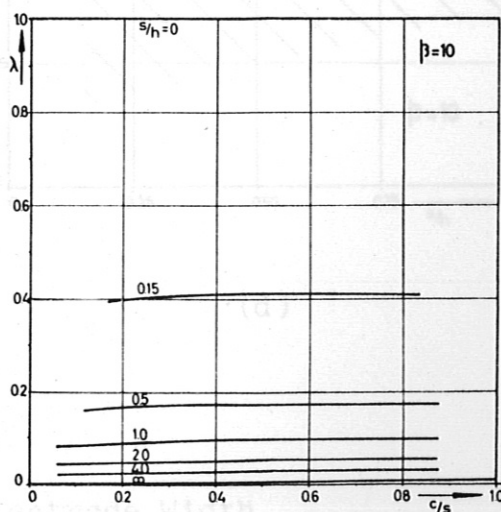
(c)



(d)



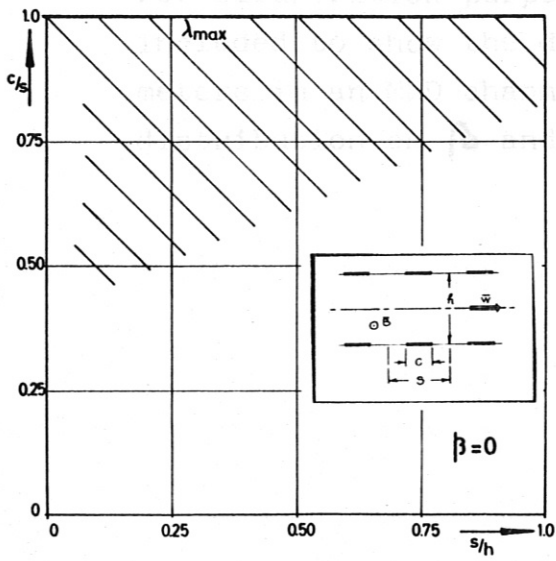
(e)



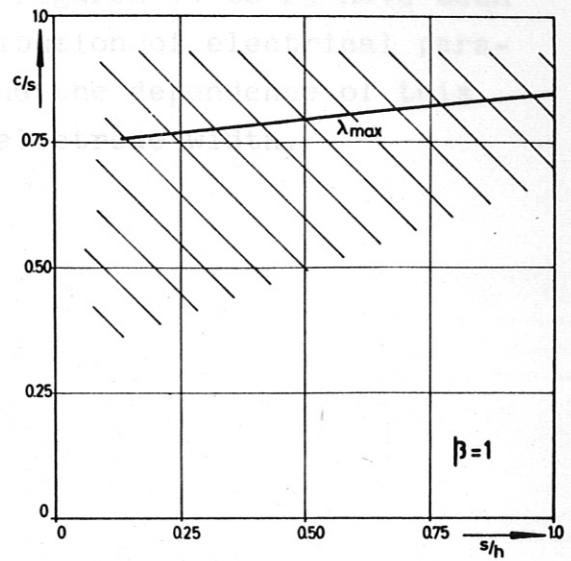
(f)

Fig. 12 Dependence of  $\lambda$  on  $c/s$

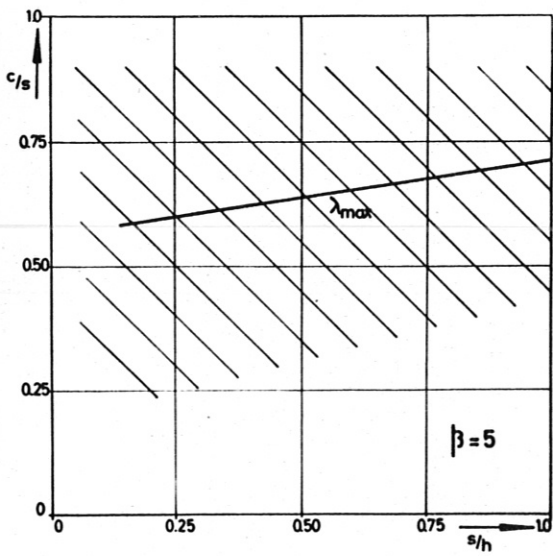
Optimum Distribution of Electrical Parameters in MFD Channel



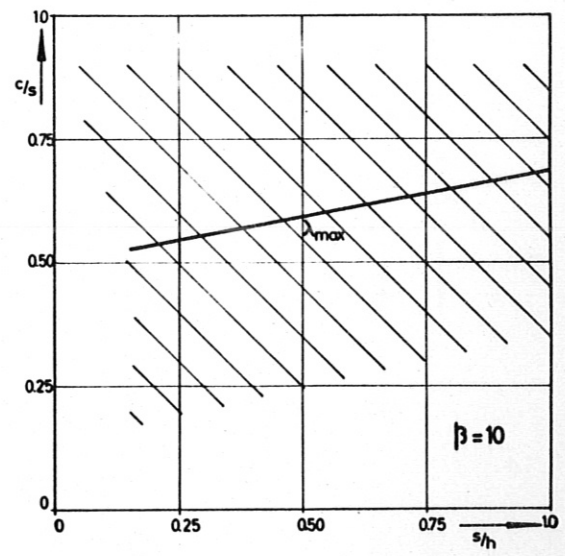
(a)



(b)



(c)



(d)

Fig. 13 Optimum Electrode Width

### 5.2 Distribution of Electrical Parameters in MHD Channel

For illustration purposes, Figures 14 to 25 have been included to show the distribution of electrical parameters in an MHD channel and the dependence of this distribution on  $\beta$  and on electrode width.

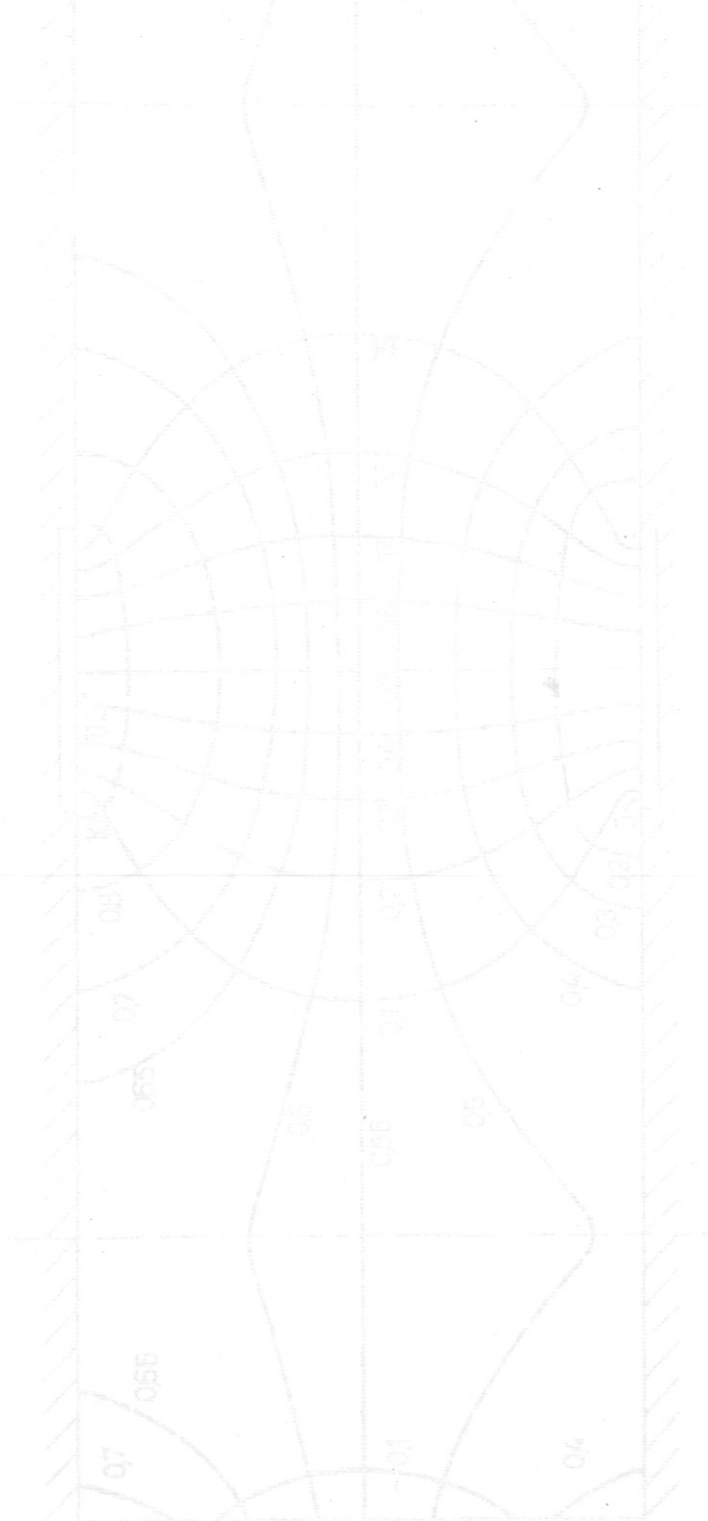


Fig. 14. Distribution of  $\chi$  and  $\psi$  for  $\beta = 2$ ,  $q/a = 0.25$ ,  $\beta = 2$ .  
—  $\chi$  constant —  $\psi$  constant

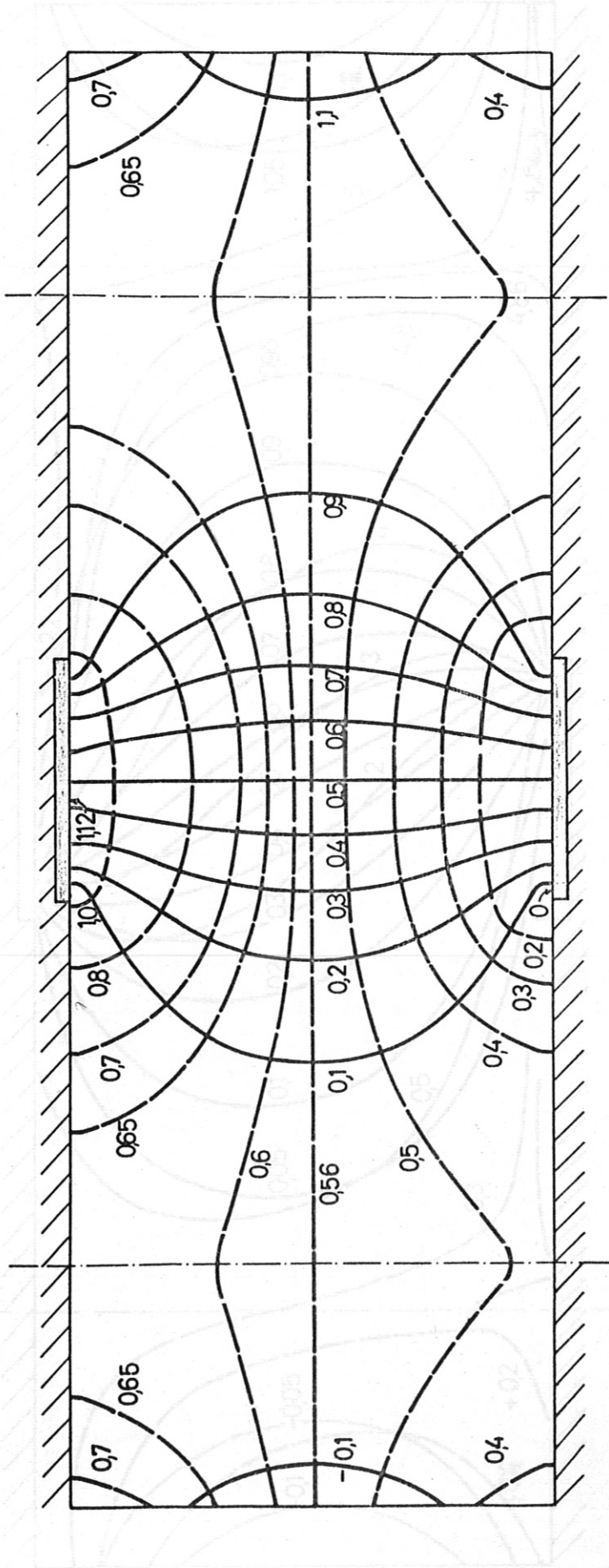


Fig. 14 Distribution of  $\gamma$  and  $\varphi^*$  for  $s/h = 2$ ,  $c/s = 0.25$ ,  $\beta = 0$   
—  $\gamma$  constant      - - -  $\varphi^*$  constant

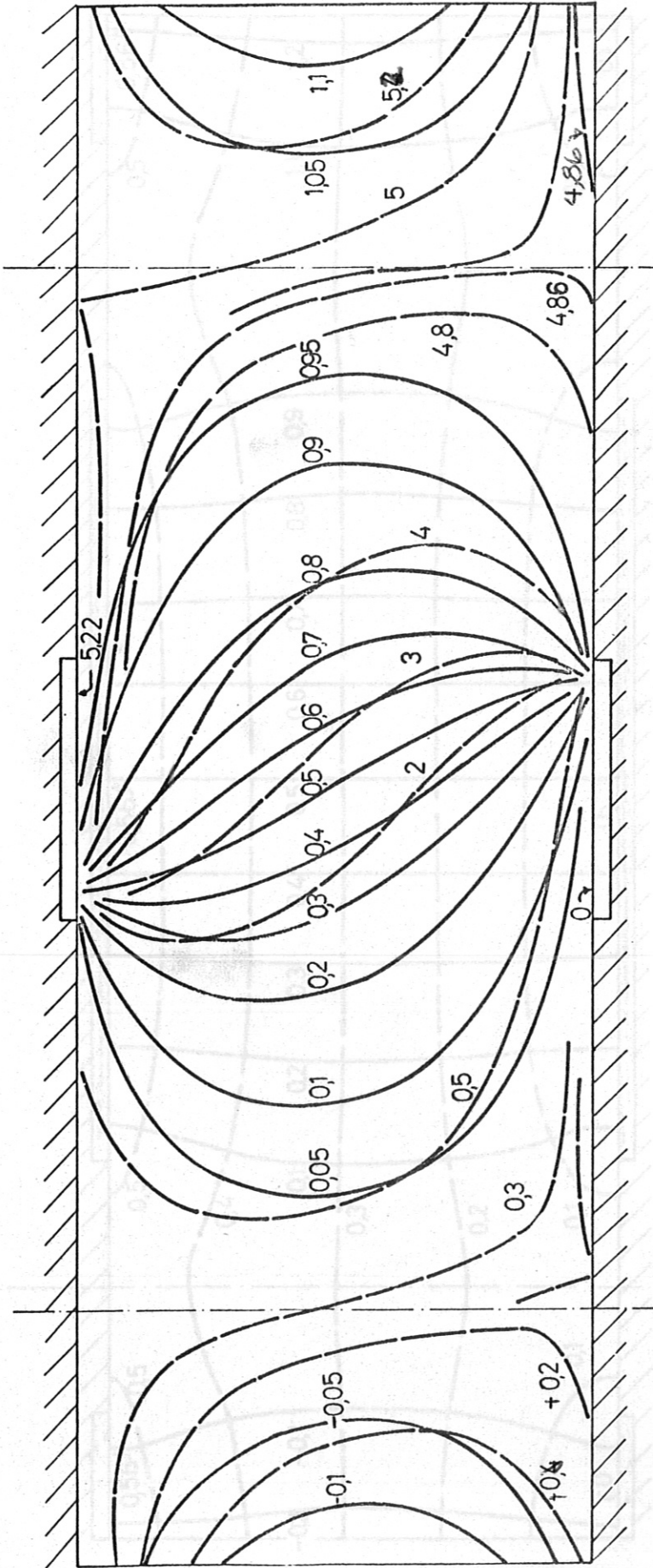


Fig. 15 Distribution of  $\gamma$  and  $\varphi^*$  for  $s/h = 2$ ,  $c/s = 0.25$ ,  $\beta = 5$   
—  $\gamma$  constant      - - -  $\varphi^*$  constant

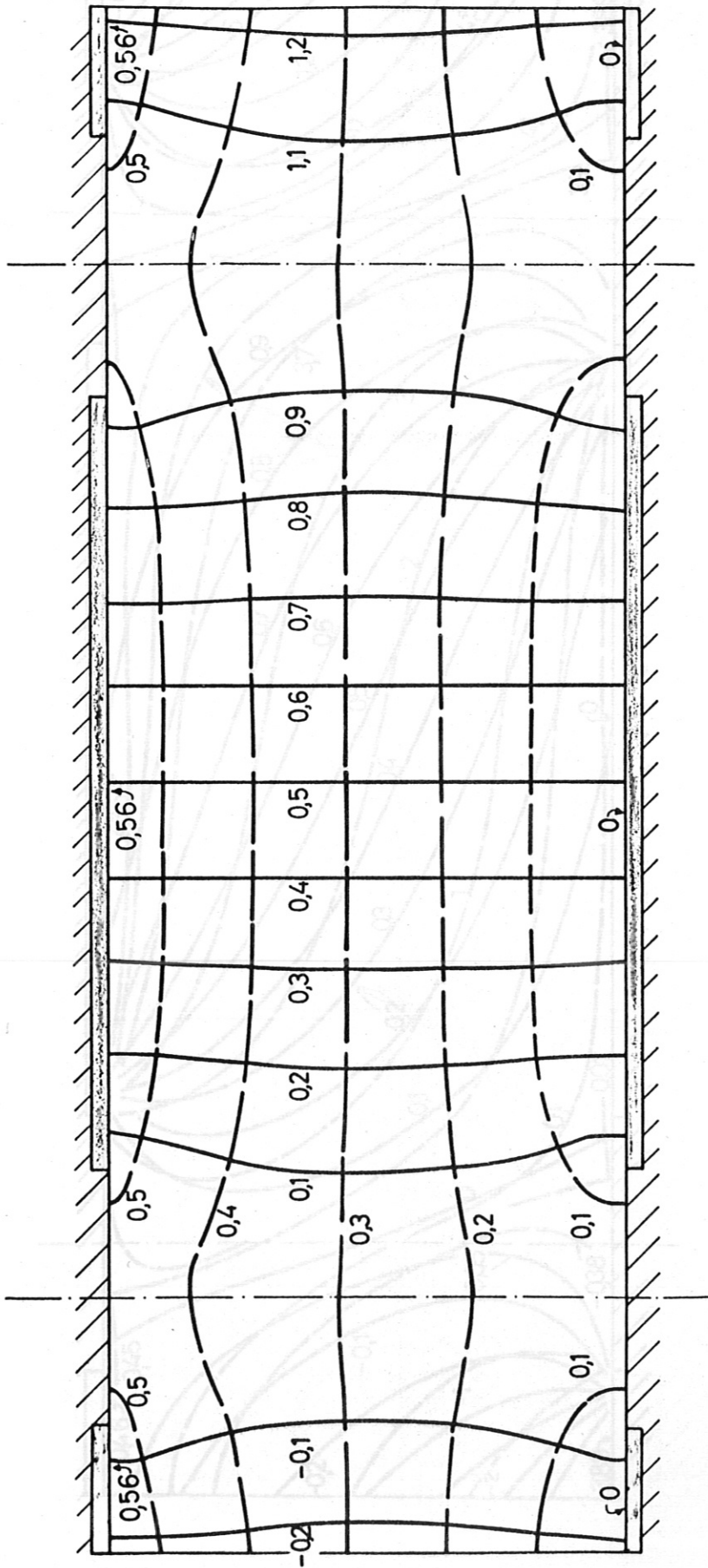


FIG. 16 Distribution of  $\gamma$  and  $\varphi^*$  for  $s/h = 2$ ,  $c/s = 0.75$ ,  $\beta = 0$   
 —  $\gamma$  constant      - - -  $\varphi^*$  constant



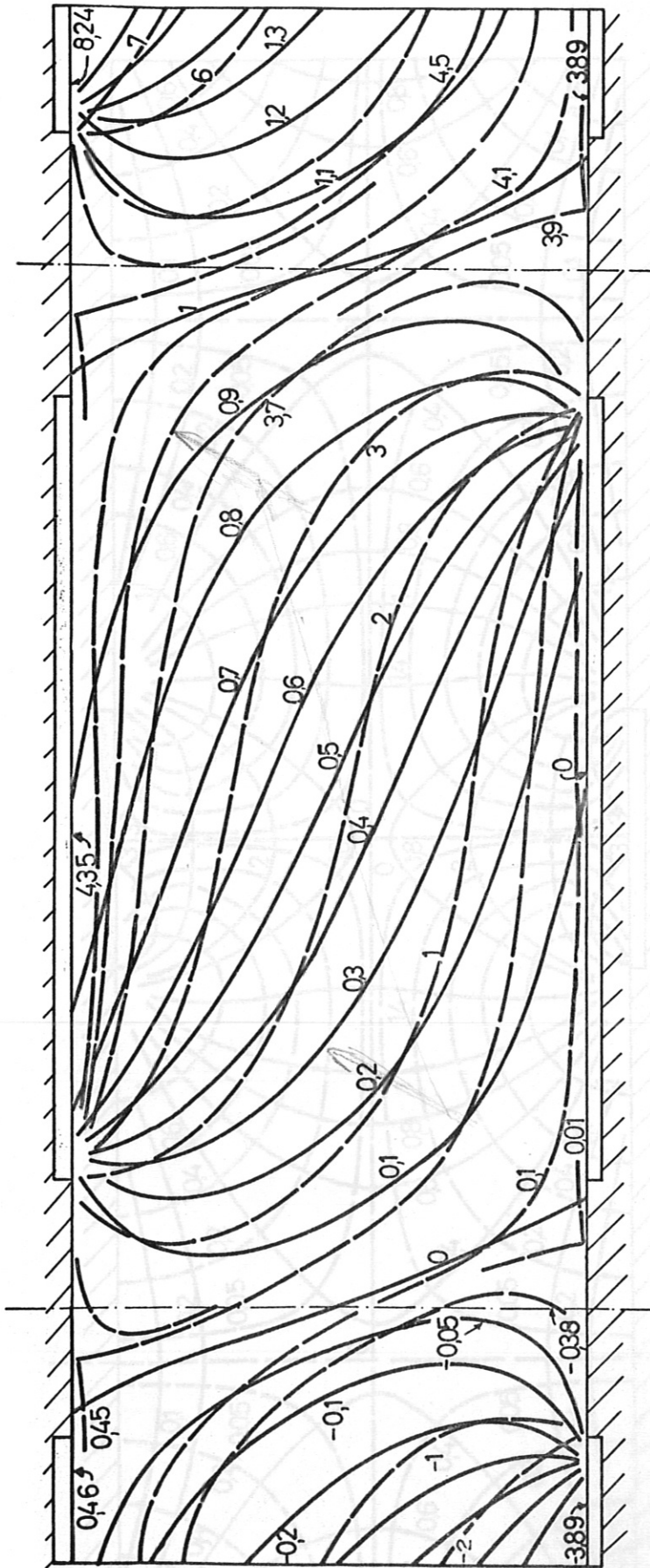


FIG. 17 Distribution of  $\gamma$  and  $\varphi^*$  for  $s/h = 2$ ,  $c/s = 0.75$ ,  $\beta = 5$

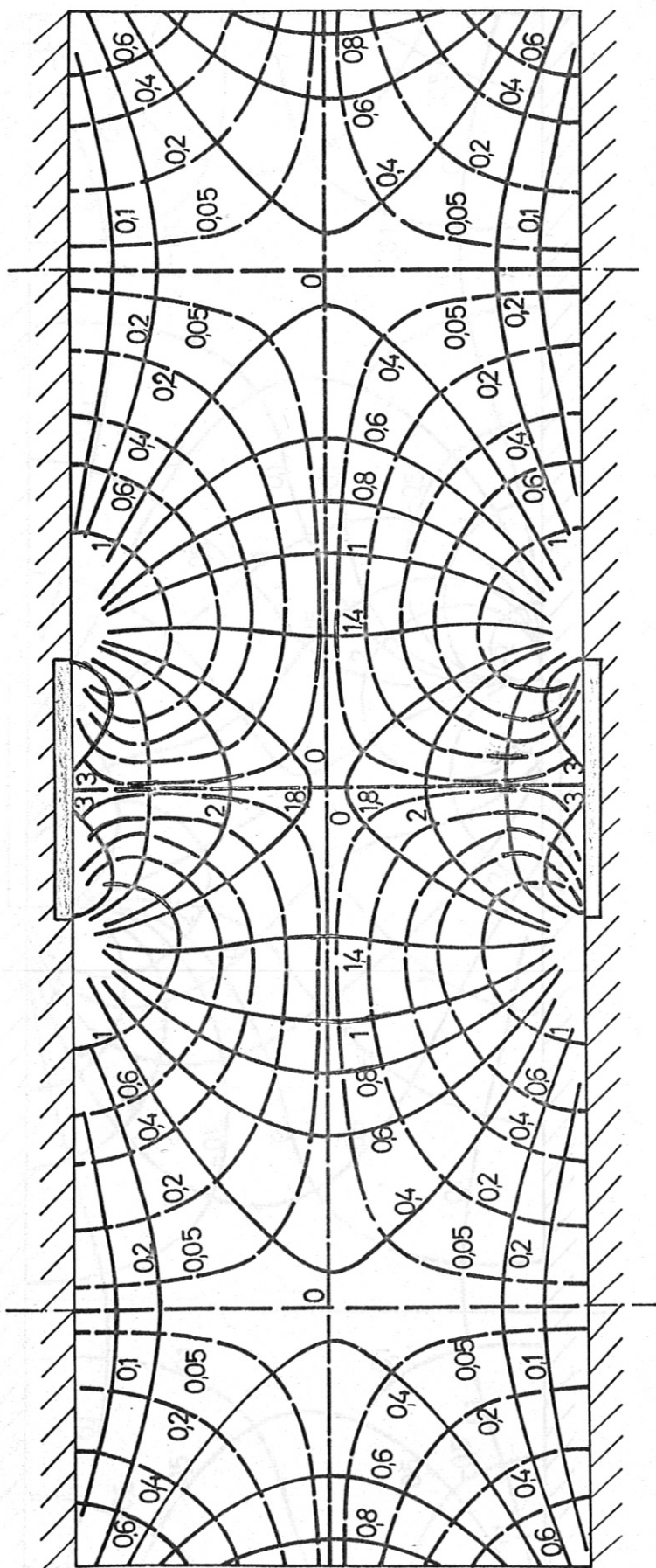


Fig. 18 Distribution of  $j_x$  and  $j_y$  for  $s/h = 2$ ,  $c/s = 0.25$ ,  $\beta = 0$   
---  $j_x$  constant      - - -  $j_y$  constant

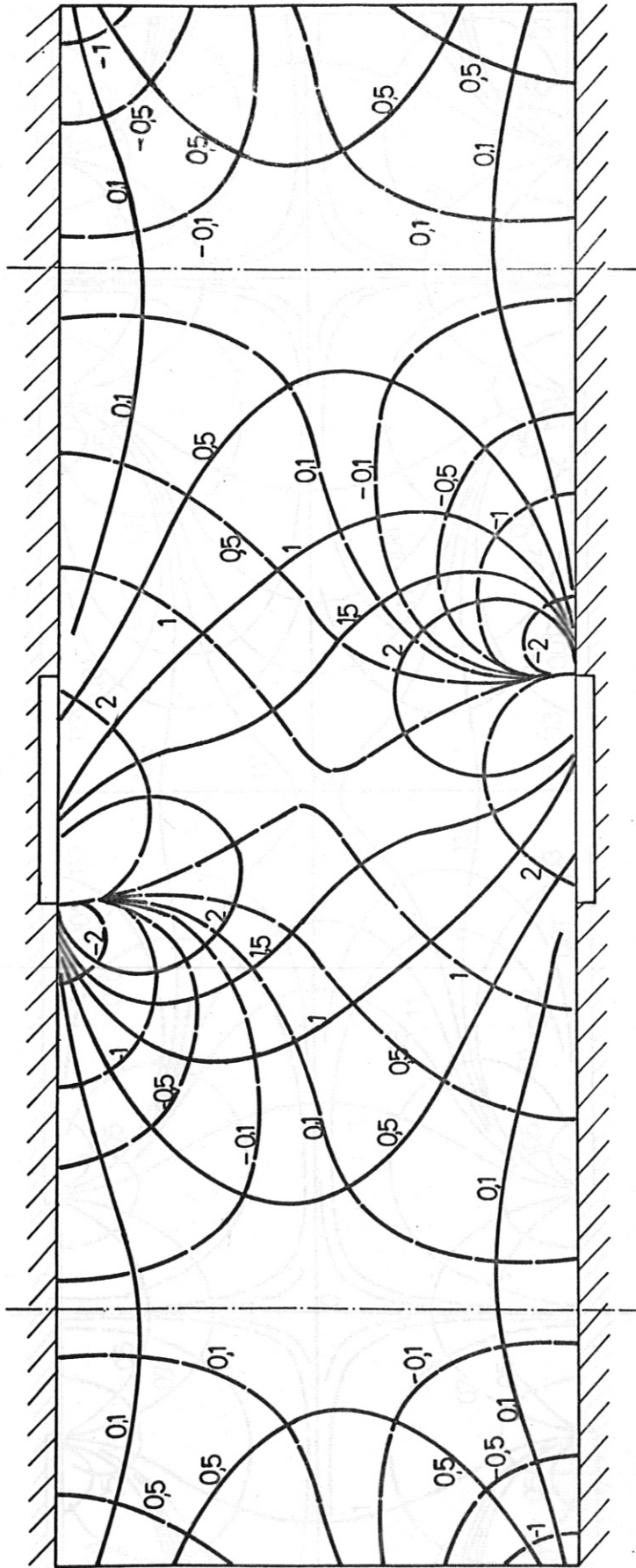


Fig. 19 Distribution of  $j_x$  and  $j_y$  for  $s/h = 2$ ,  $c/s = 0.25$ ,  $\beta = 5$   
---  $j_x$  constant      —  $j_y$  constant

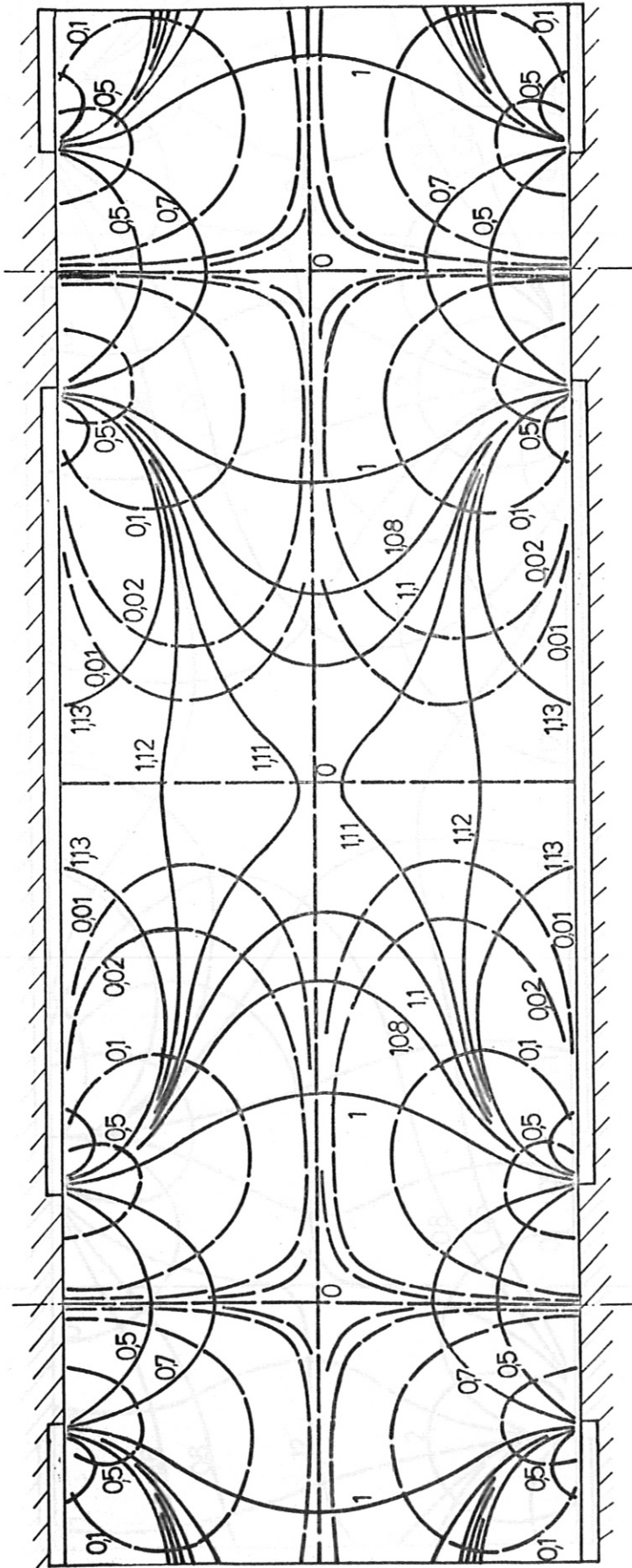


Fig. 20 Distribution of  $j_x$  and  $j_y$  for  $s/h = 2$ ,  $c/s = 0.75$ ,  $\beta = 0$   
 ---  $j_x$  constant    ———  $j_y$  constant

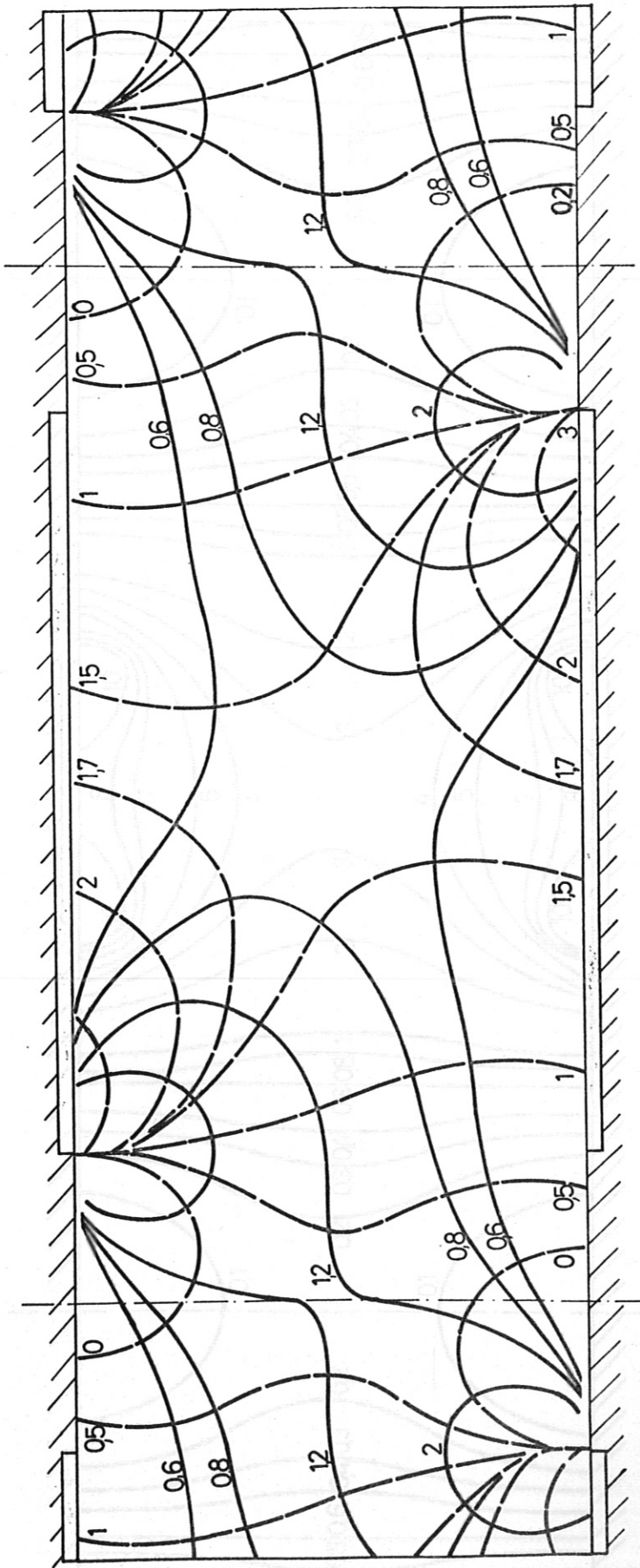


Fig. 21 Distribution of  $j_x^*$  and  $j_y^*$  for  $s/h = 2$ ,  $c/s = 0.75$ ,  $\beta = 5$   
---  $j_x^*$  constant      —  $j_y^*$  constant

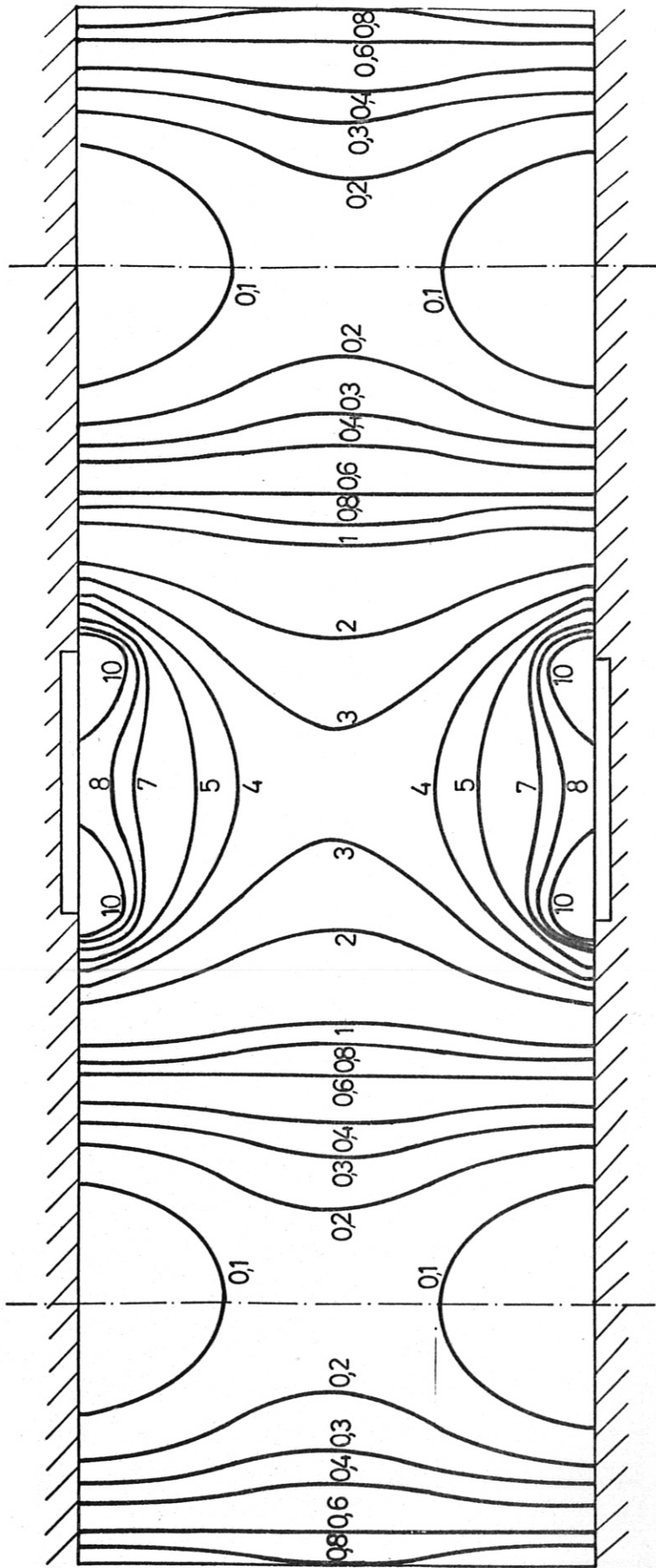


Fig. 22 Distribution of  $q$  for  $s/h = 2$ ,  $c/s = 0.25$ ,  $\beta = 0$

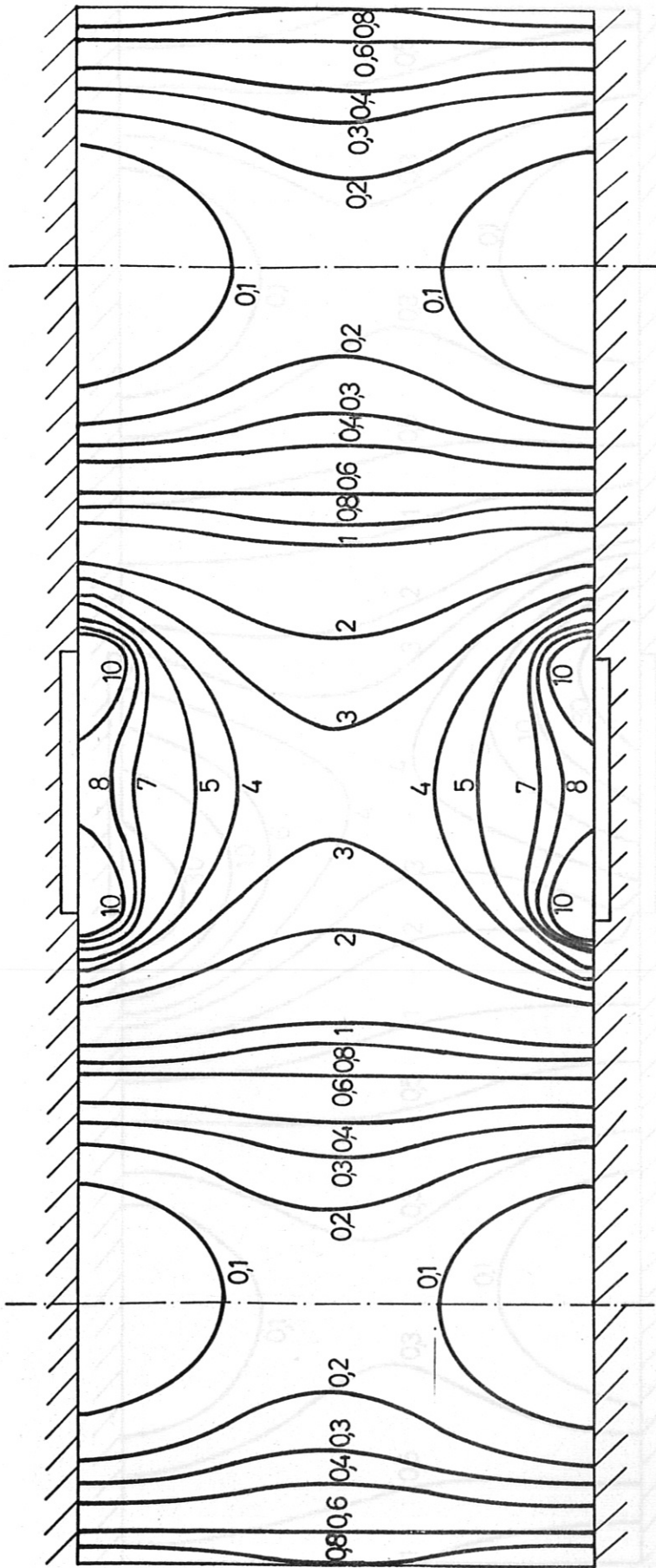


Fig. 22 Distribution of  $q$  for  $s/h = 2$ ,  $c/s = 0.25$ ,  $\beta = 0$

Fig. 23 Distribution of  $q$  for  $s/h = 2$ ,  $c/s = 0.25$ ,  $\beta = 1$

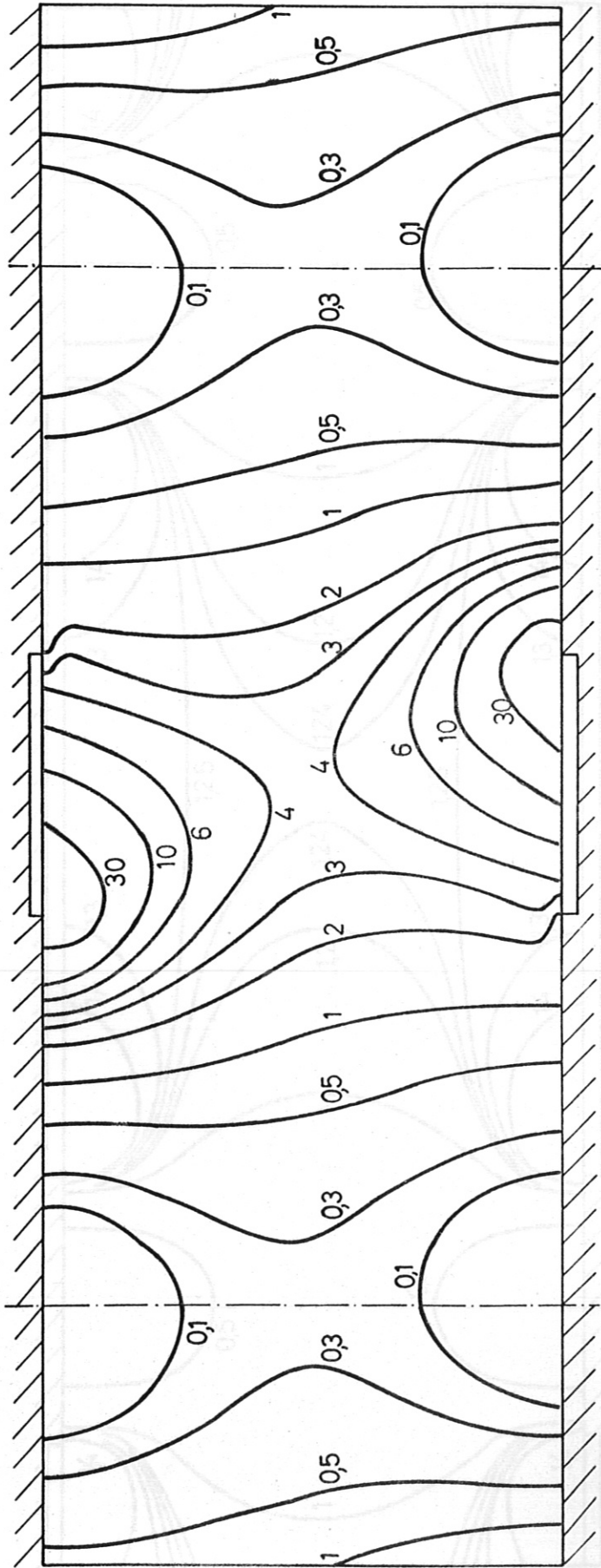


Fig. 23 Distribution of  $q$  for  $s/h = 2$ ,  $c/s = 0.25$ ,  $\beta = 5$



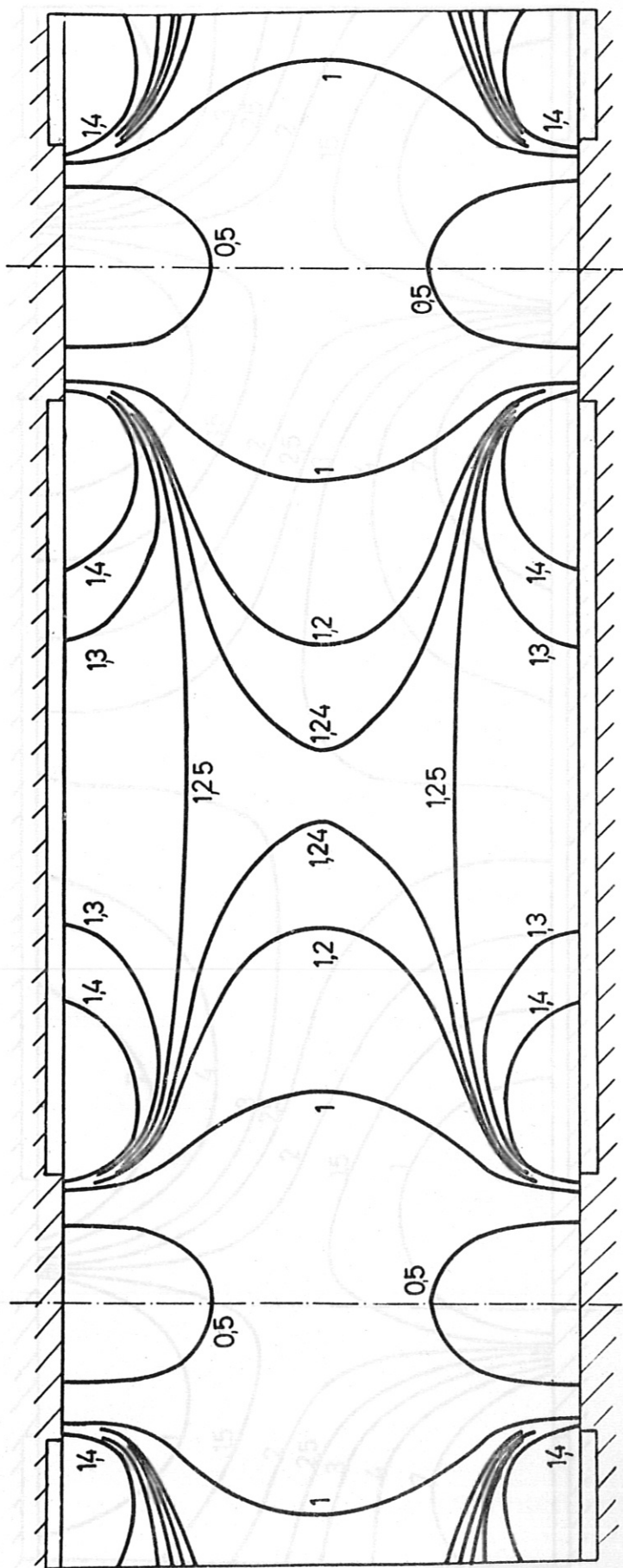


Fig. 24 Distribution of  $q$  for  $s/h = 2$ ,  $c/s = 0.75$ ,  $\beta = 0$

5.3 Current Distribution Along Electrode

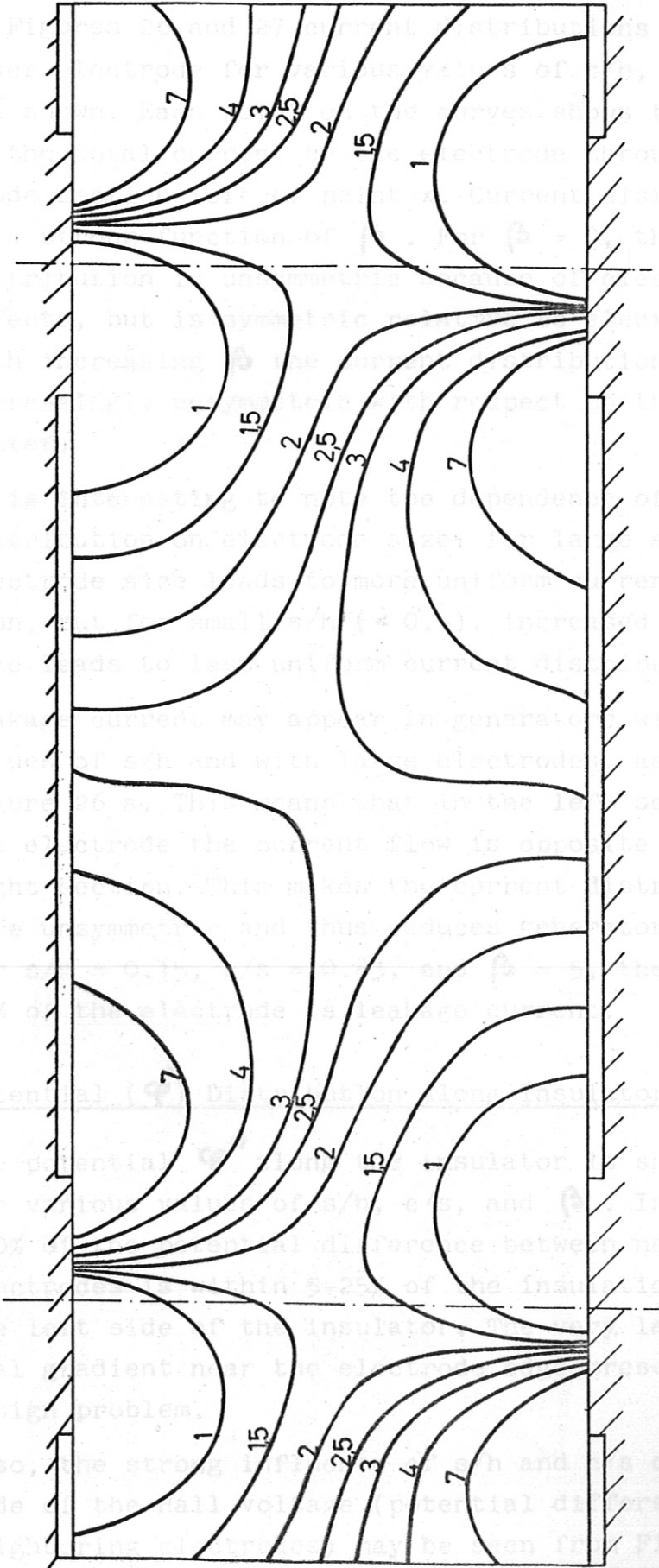


Fig. 25 Distribution of  $q$  for  $s/h = 2$ ,  $c/s = 0.75$ ,  $\beta = 5$

5.4 Potential

In Fig. 25, the distribution of current density  $q$  is shown along the lower electrode for different values of the parameter  $s/h$ ,  $c/s$ , and  $\beta$ . The fraction of the total current carried by the electrode is shown in the table. The current density is highest near the corners of the electrode segments and lowest in the middle of the segments. As  $s/h$  increases, the current density becomes more concentrated at the corners. The current density is also higher for larger values of  $\beta$  and  $c/s$ .

The potential distribution is shown in Fig. 26. The potential is highest at the corners of the electrode segments and lowest in the middle of the segments. As  $s/h$  increases, the potential becomes more concentrated at the corners. The potential is also higher for larger values of  $\beta$  and  $c/s$ .

The potential distribution is shown in Fig. 26. The potential is highest at the corners of the electrode segments and lowest in the middle of the segments. As  $s/h$  increases, the potential becomes more concentrated at the corners. The potential is also higher for larger values of  $\beta$  and  $c/s$ .

### 5.3 Current Distribution Along Electrode

In Figures 26 and 27 current distributions along the lower electrode for various values of  $s/h$ ,  $c/s$ , and  $\beta$  are shown. Each point on the curves shows the fraction of the total current to the electrode through the electrode section left of point  $x$ . Current distribution is a strong function of  $\beta$ . For  $\beta = 0$ , the current distribution is unsymmetric because of electrode end-effects, but is symmetric relative to electrode center. With increasing  $\beta$  the current distribution becomes increasingly unsymmetric with respect to the electrode center.

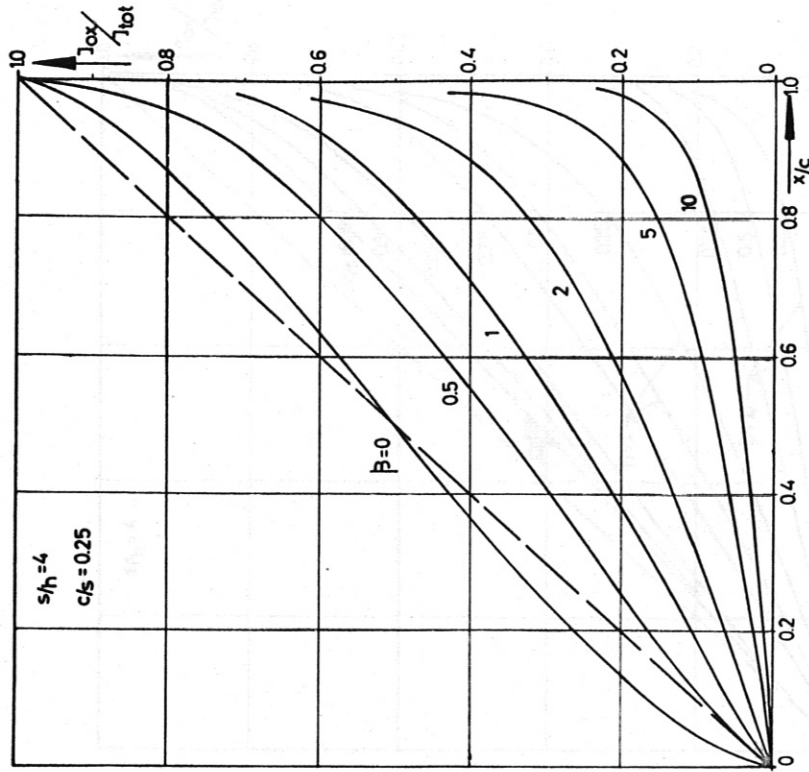
It is interesting to note the dependence of current distribution on electrode size: for large  $s/h$ , increased electrode size leads to more uniform current distribution, but for small  $s/h$  ( $< 0.5$ ), increased electrode size leads to less uniform current distribution (Fig. 26).

Leakage current may appear in generators with small values of  $s/h$  and with large electrodes, as shown in Figure 26 a. This means that in the left section of the electrode the current flow is opposite that in the right section. This makes the current distribution even more unsymmetric and thus reduces generator performance. For  $s/h = 0.15$ ,  $c/s = 0.83$ , and  $\beta = 5$ , the current in 50% of the electrode is leakage current.

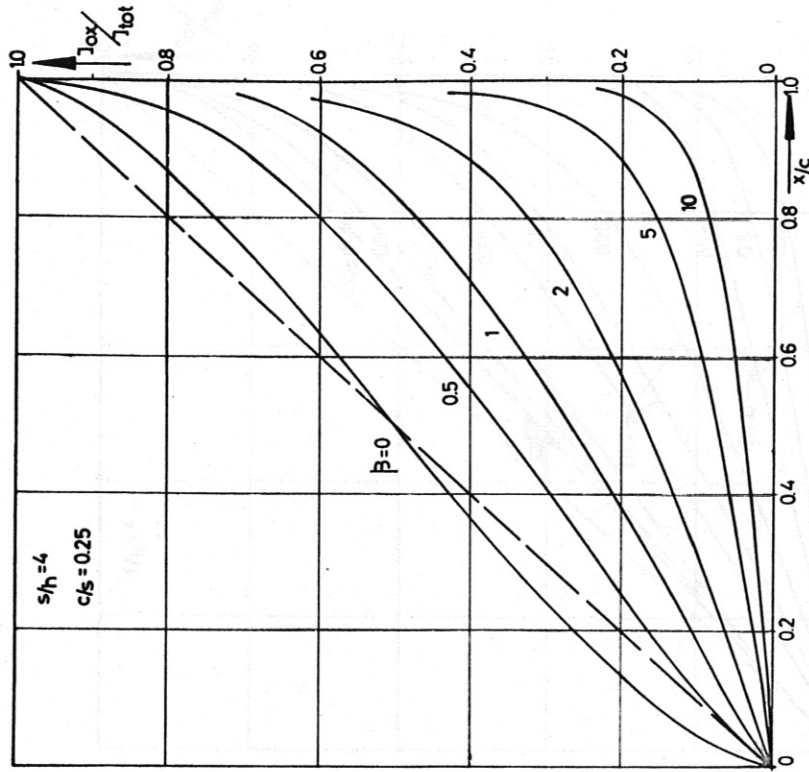
### 5.4 Potential ( $\varphi^*$ ) Distribution Along Insulator

The potential  $\varphi^*$  along the insulator is shown in Fig. 28 for various values of  $s/h$ ,  $c/s$ , and  $\beta$ . In all cases, 100% of the potential difference between neighboring electrodes is within 5-25% of the insulation width at the left side of the insulator. The very large potential gradient near the electrode edge presents a severe design problem.

Also, the strong influence of  $s/h$  and  $c/s$  on the magnitude of the Hall voltage (potential difference between neighboring electrodes) may be seen from Figures 28a and b, respectively.



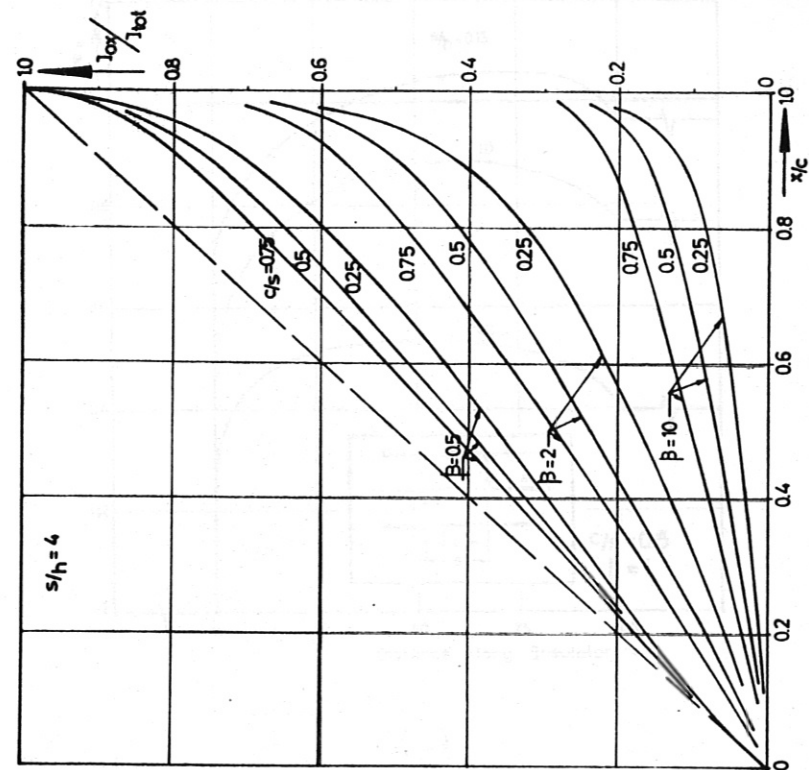
(a)



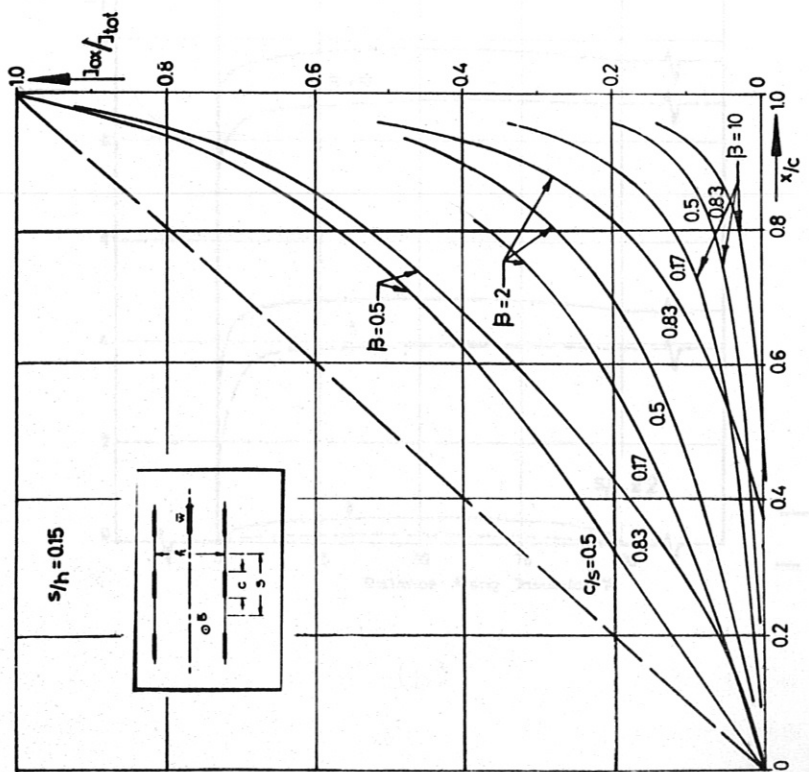
(b)

Fig. 26 Current Distribution Along Electrode for  $s/h = 0.15$ ,  $c/s = 0.83$  and  $s/h = 4$ ,  $c/s = 0.25$

$J_{ox}/J_{tot}$  = Fraction of total current to electrode left of point indicated  
 $x/c$  = Fraction of distance along electrode from left electrode edge

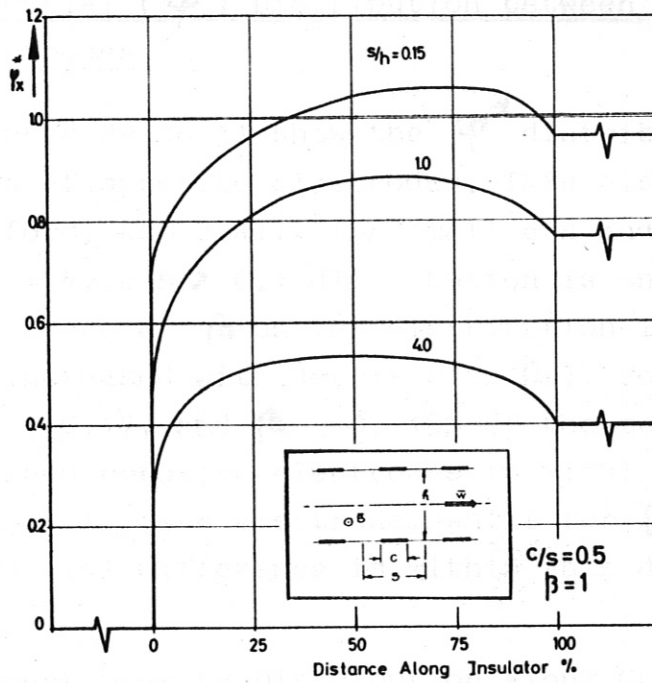


(a)

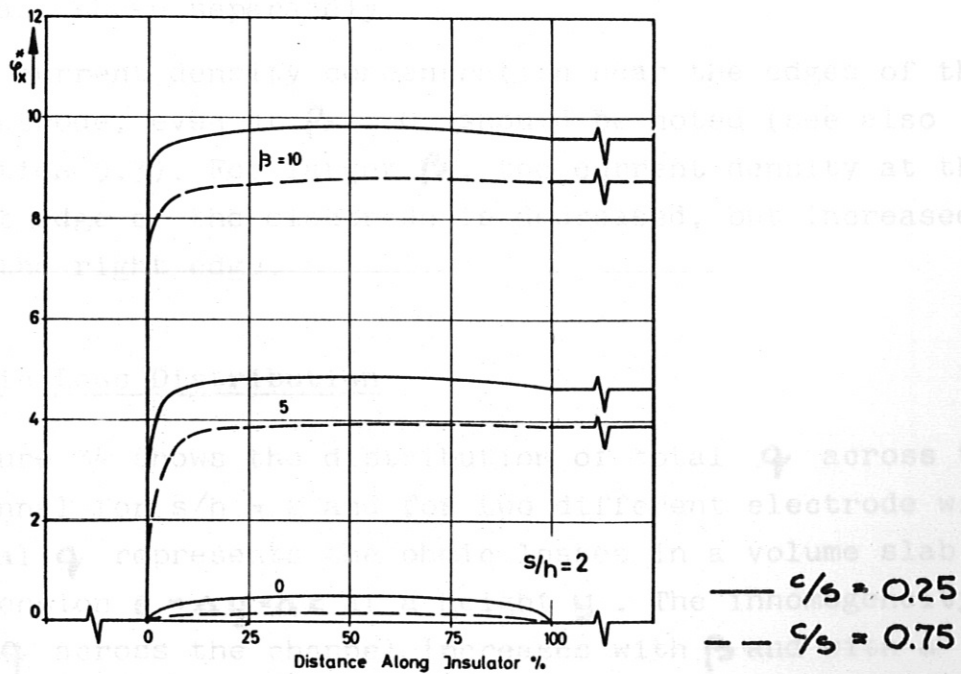


(b)

Fig. 27 Current Distribution Along Electrode for  $c/s = 0.25$  to  $0.83$   
For notation see p. 49



(a)



(b)

Fig. 28  $\phi^*$  Along Electrode and Insulator Wall.

### 5.5 Potential ( $\varphi^*$ ) Distribution between Centers of Opposite Electrodes

Figures 29 to 31 show the  $\varphi^*$  distribution between centers of opposite electrodes. This distribution is non-uniform, especially for small  $c/s$  and small  $s/h$  (for  $s/h = 4$ ,  $c/s > 0.1$  distribution is uniform). Also, the influence of  $\beta$  on the distribution is strong (uniformity is increased with decrease in  $\beta$ ). For  $s/h = 0.15$ ,  $c/s = 0.17$ , and  $\beta = 0$ , 10% of the potential difference between opposite electrodes is within 5% of the channel height at each electrode, while for  $\beta = 10$ , 30% of the potential difference is within this distance.

### 5.6 Current Density Distribution Along Channel Wall

Figures 32 and 33 show current density along the electrode and insulator. The case of  $s/h = 2$  is shown with large (Fig. 32) and small (Fig. 33) electrodes.  $j_x$  and  $j_y$  are shown separately.

The current density concentration near the edges of the electrode, even at  $\beta = 0$ , should be noted (see also Section 5.3). For larger  $\beta$ , the current density at the left edge of the electrode is decreased, but increased at the right edge.

### 5.7 Ohmic Loss Distribution

Figure 34 shows the distribution of total  $q$  across the channel for  $s/h = 2$  and for two different electrode widths. Total  $q$  represents the ohmic losses in a volume slab of dimension  $s \times \Delta y \times \Delta z$  at a height  $y$ . The inhomogeneity of  $q$  across the channel increases with  $\beta$  and with a decrease in electrode size.

In Figure 35 is shown the  $q$ -distribution along the channel wall.  $q$  along the wall is defined as  $\frac{dq}{dV} = \frac{dq}{dy \Delta x \Delta z} = \frac{dq}{dy}$  with  $\Delta x \Delta z = 1$ . Fig. 36 shows  $q$  for large  $c/s$ .

Ohmic losses determine electron heating to a temperature above the gas temperature. Thus, consideration of electron

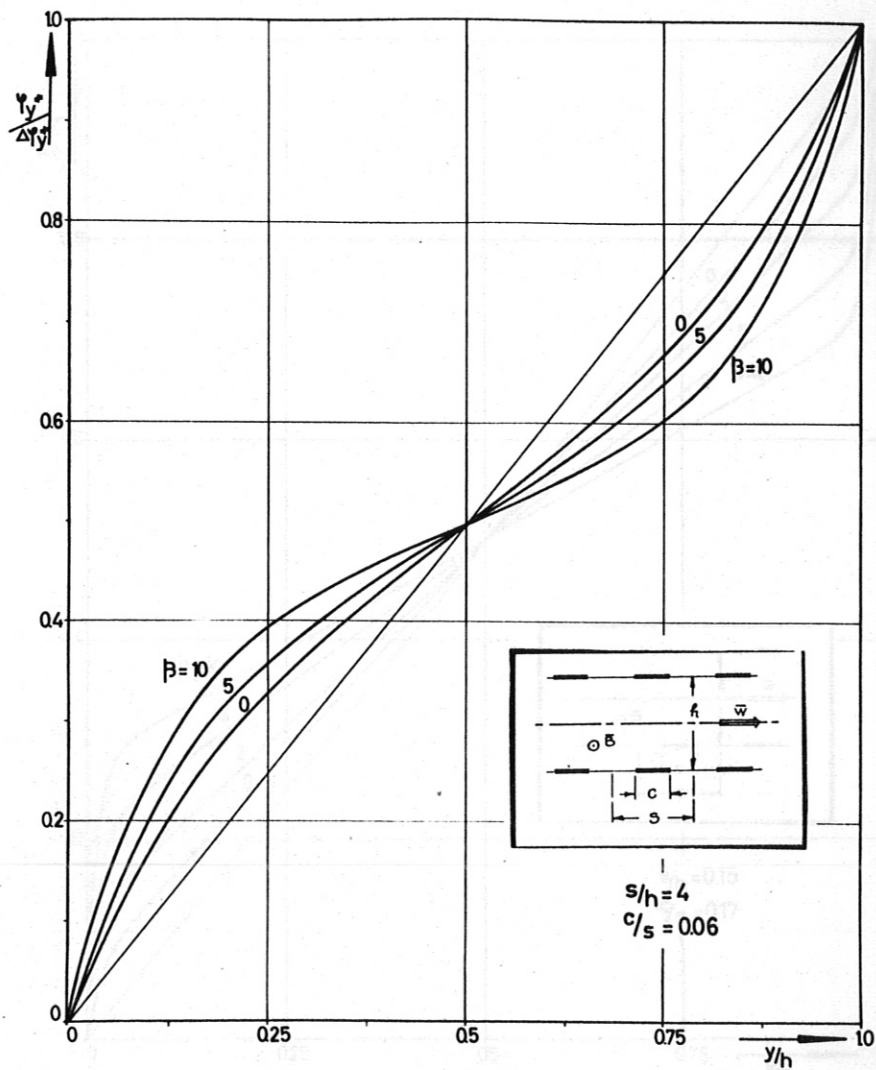


Fig. 29  $\varphi_y^* / \Delta\varphi_y^*$  Between Centers of Opposite Electrodes  
for  $s/h = 4$ ,  $c/s = 0.06$



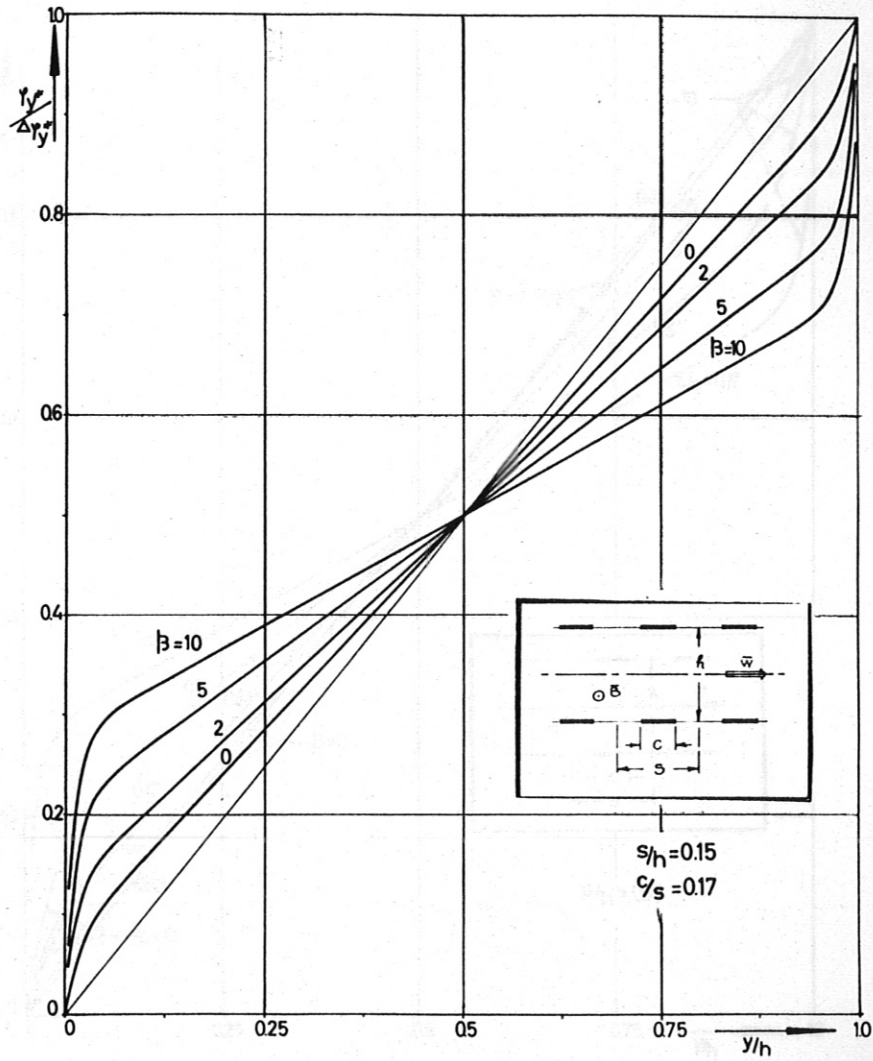


Fig. 30  $\frac{\varphi_y^*}{\Delta\varphi_y^*}$  Between Centers of Opposite Electrodes for  $s/h = 0.15, c/s = 0.17$

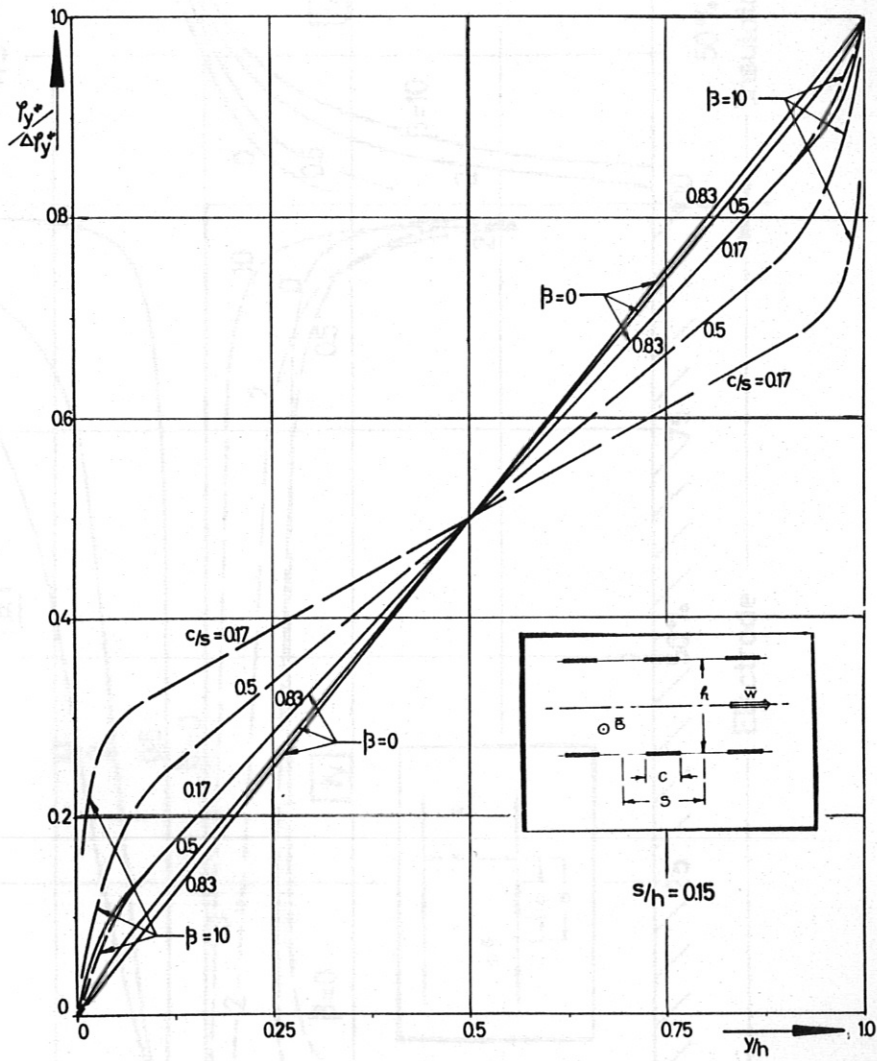


Fig. 31  $\frac{\varphi_y^*}{\Delta \varphi_y^*}$  Between Centers of Opposite Electrodes for  $s/h = 0.15$ ,  $c/s$  from 0.17 to 0.83

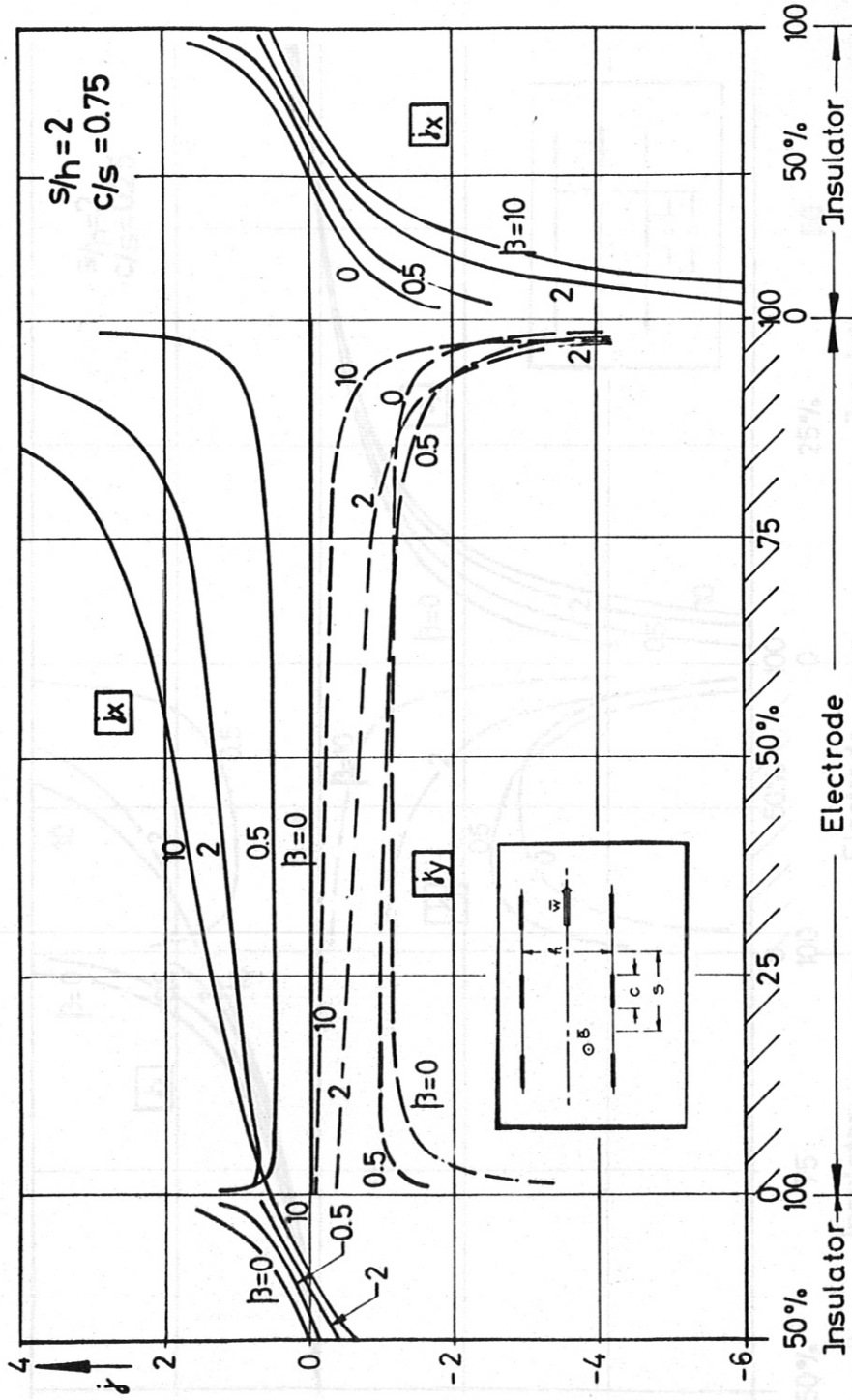


Fig. 32  $j_x$  and  $j_y$  Along Electrode and Insulator Wall for  $s/h = 2$ ,  $c/s = 0.25$

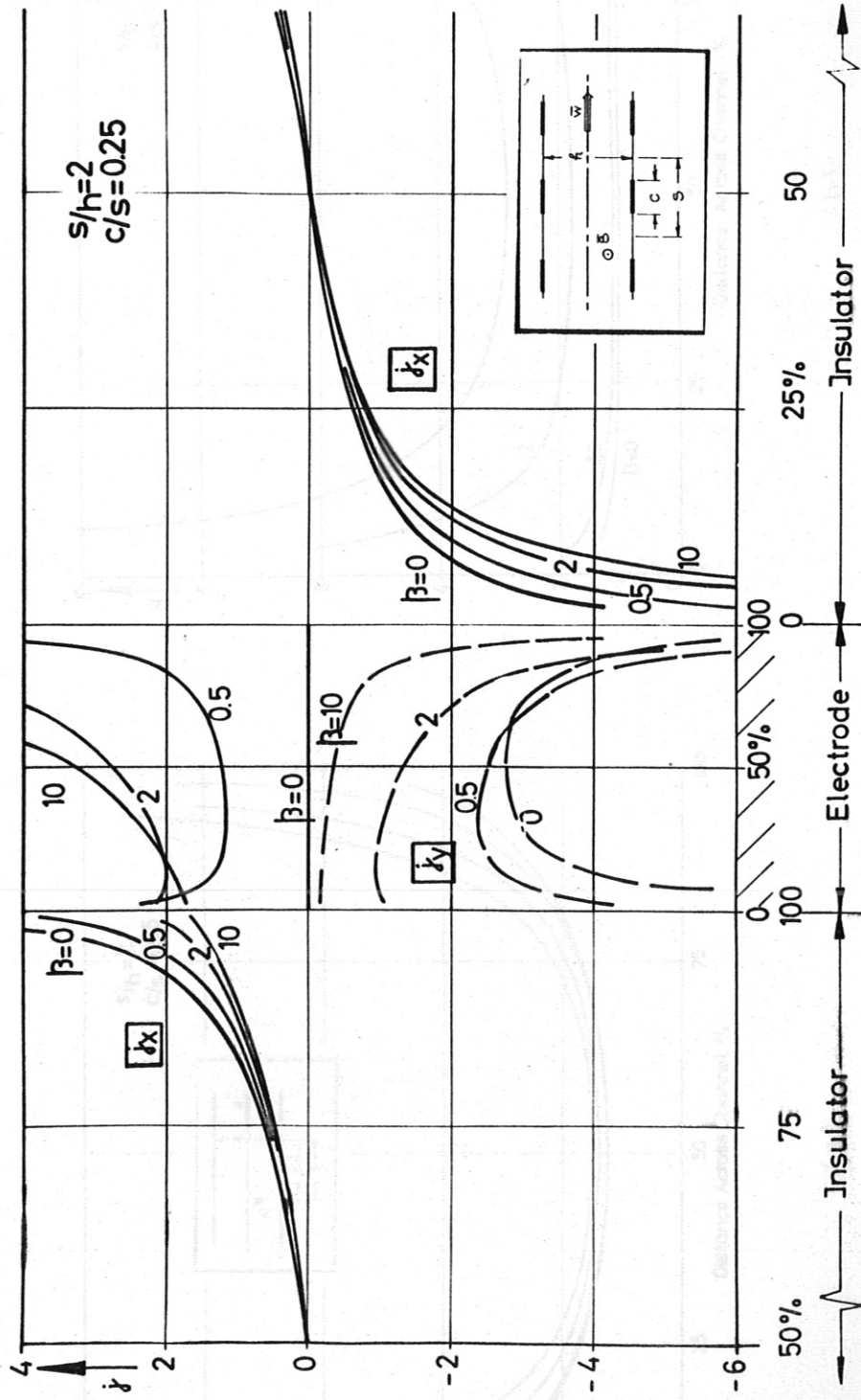
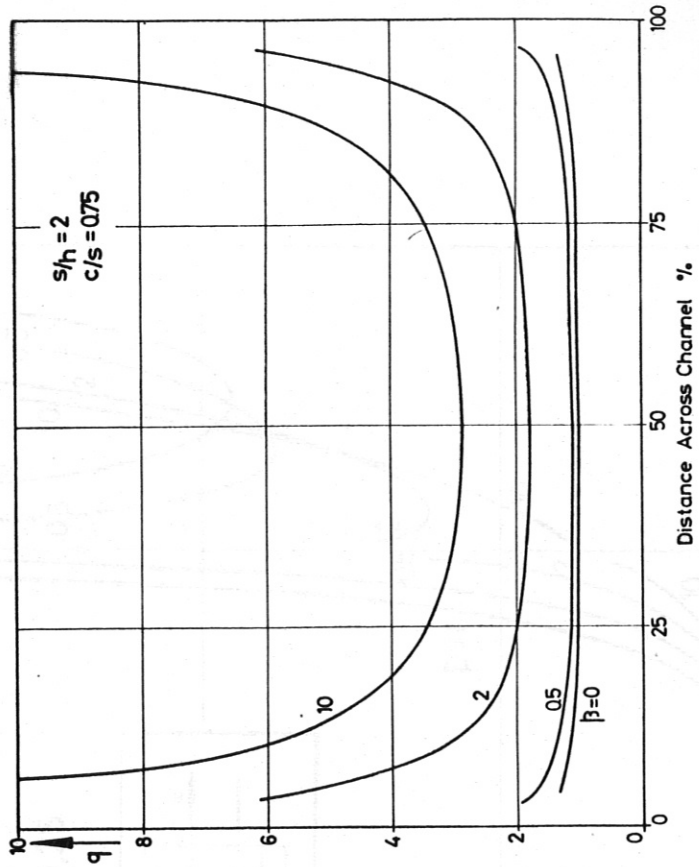
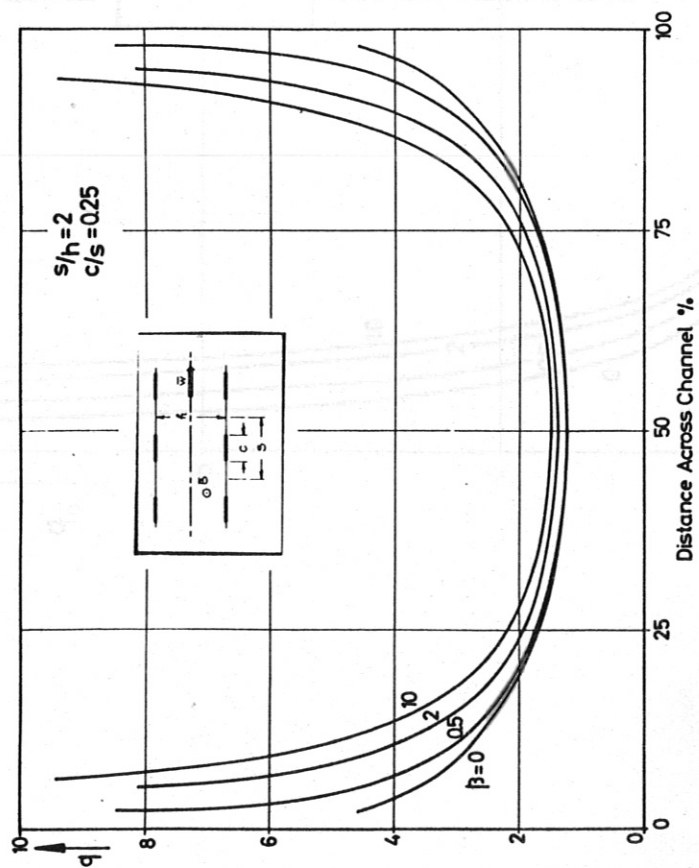


FIG. 33  $j_x$  and  $j_y$  Along Electrode and Insulator Wall for  $s/h = 2$ ,  $c/s = 0.75$



(a)



(b)

Fig. 34 Total  $q$  Across Channel for  $s/h = 2$  and  $c/s = 0.25$  and  $0.75$

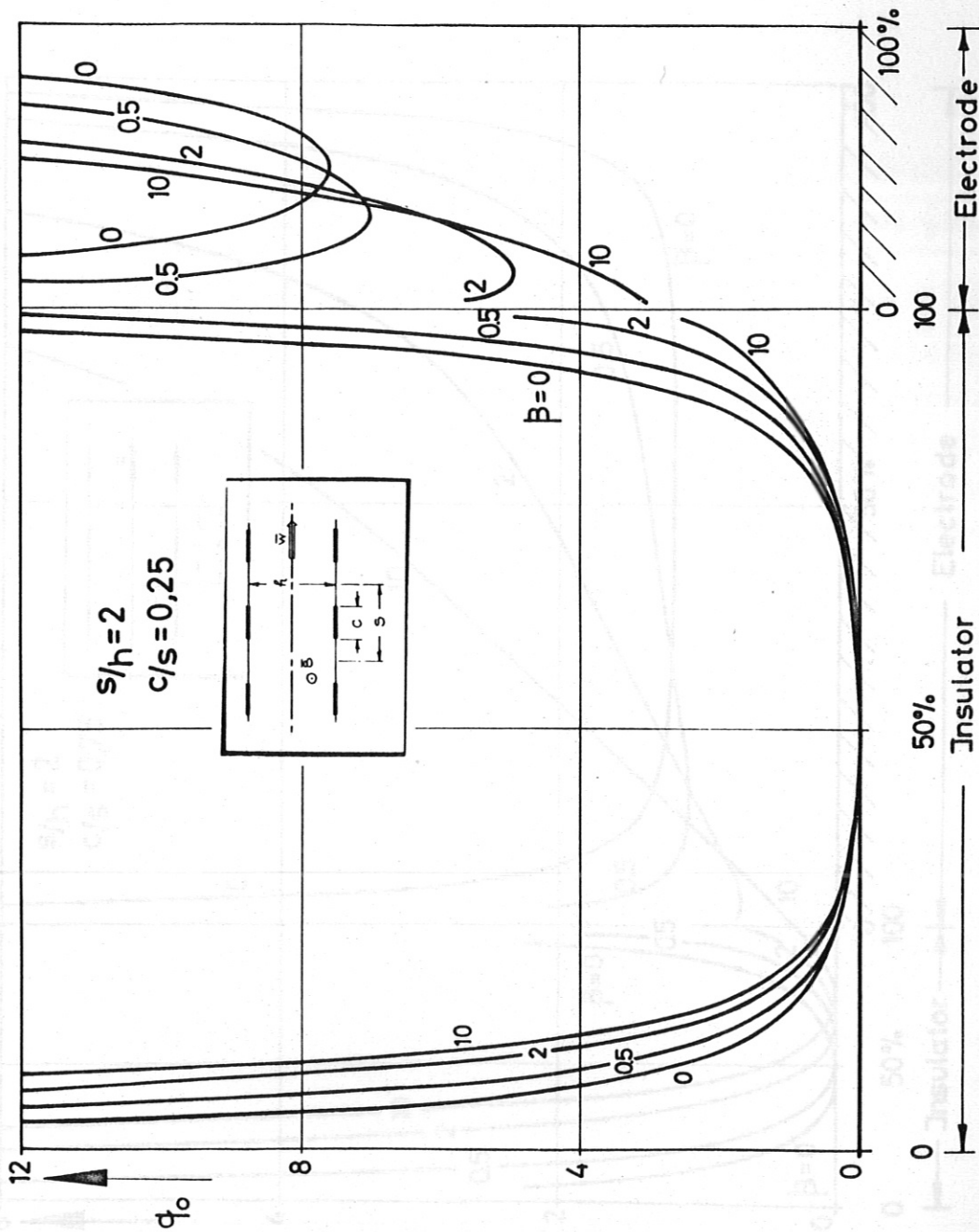


FIG. 35  $q$  Along Electrode and Insulation Wall for  $s/h = 2$ ,  $c/s = 0.25$

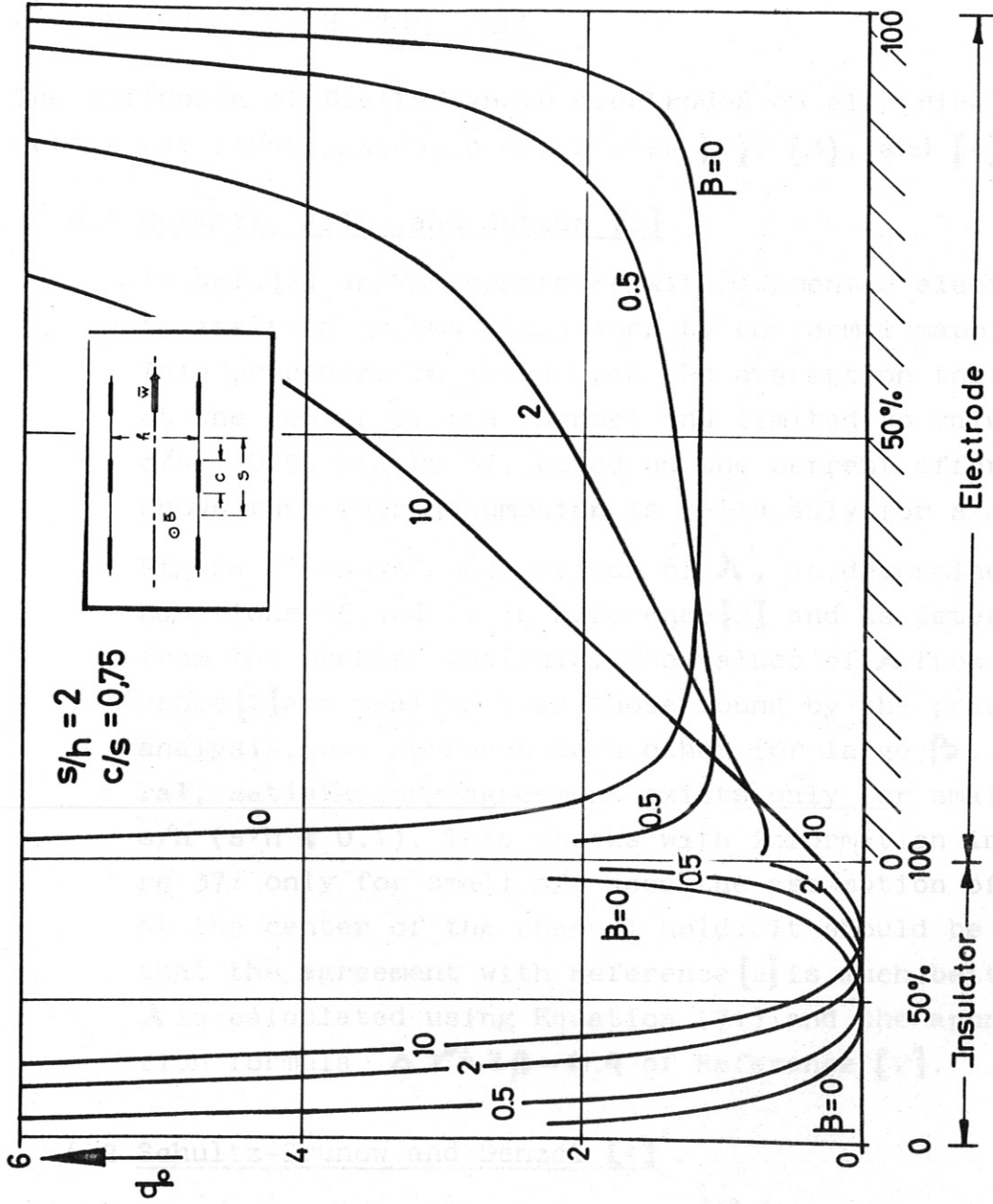


Fig. 36 Along Electrode and Insulator Wall for  $s/h = 2$ ,  $c/s = 0.75$

heating must take into account the large gradient of  $q$  in the channel. Electron heating causes a local increase in electrical conductivity. The result is a redistribution of all electrical parameters.

## 6. COMPARISON WITH OTHER WORK

The influence of finite-length electrodes on electrical parameters was investigated in References [2], [3], and [4].

### 6.1 Hurwitz, Kilb, and Sutton [2]

In Ref. [2] an MHD generator with segmented electrodes is analyzed in two-dimensions by conformal mapping. This procedure is based upon the assumption that  $j_x = 0$  at the center of the channel and limited to values of  $c/s = 0.5$ . Figure 37, based on the current effort, shows that this assumption is valid only for  $s/h \ll 1$ .

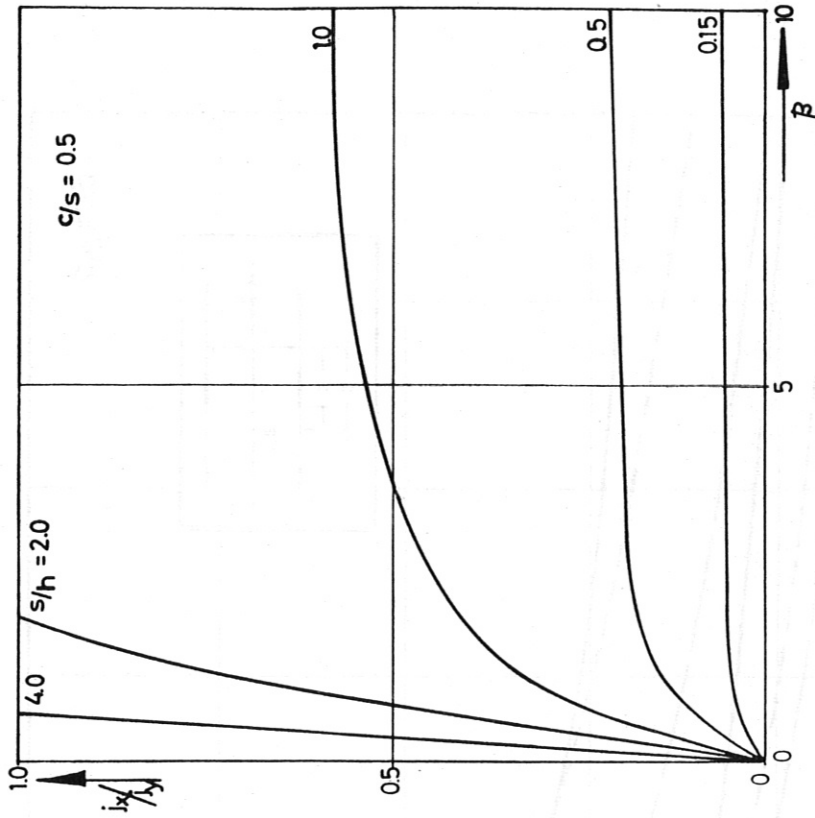
Figure 38 shows a comparison of  $\lambda$ , as determined from Equations 65 and 71 in Reference [2] and as determined from the present analysis. The values of  $\lambda$  from Reference [2] are smaller than those found by the present analysis, but approach each other for large  $\beta$ . In general, satisfactory agreement exists only for small  $s/h$  ( $s/h < 0.1$ ). This checks with information in Figure 37: only for small  $s/h$  does the assumption of  $j_x = 0$  at the center of the channel hold. It should be noted that the agreement with Reference [2] is much better when  $\lambda$  is calculated using Equation (71) and the approximation formula  $\Delta \gamma = 2\beta - 0.4$  of Reference [2].

### 6.2 Schultz-Grunow and Denzel [4]

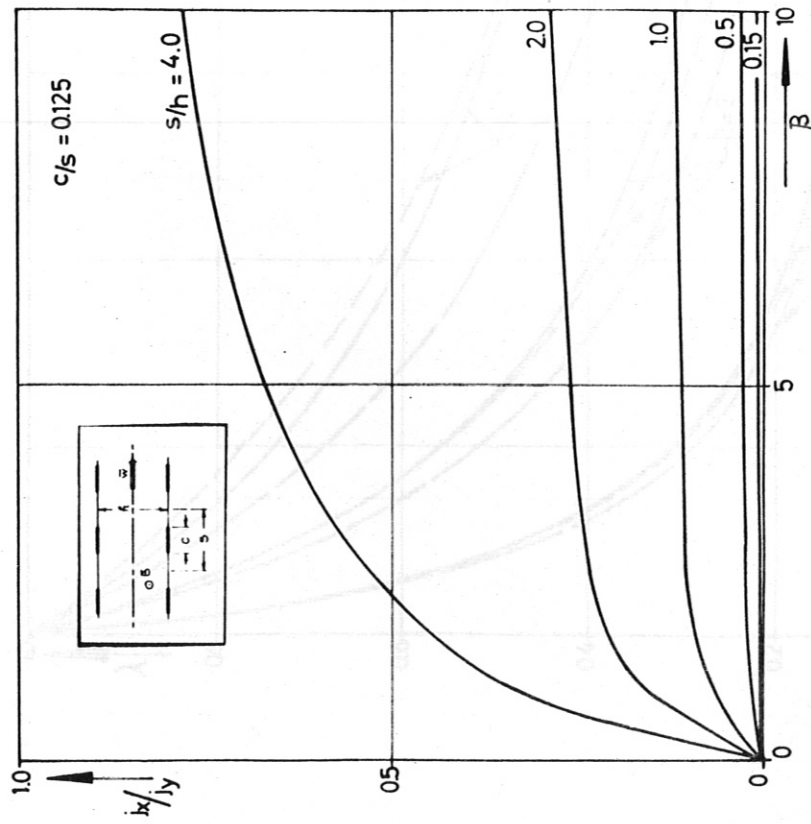
The approach used in Reference [4] is similar to that used in Reference [2]; both are based on conformal mapping. A direct comparison of  $\lambda$ -values is not possible, since the data presented in Reference [4] is only in the form of increased internal resistance at  $\beta > 0$  relative to that at  $\beta = 0$ .

However, values for  $R_\beta / R_{\beta=0}$  were calculated from present





(a)



(b)

Fig. 37  $i_x/j_y$  at Center of Section for  $c/s = 0.5$  and  $0.125$

— Present analysis  
 — Ref. [2], exact values — Ref. [2], approx. values

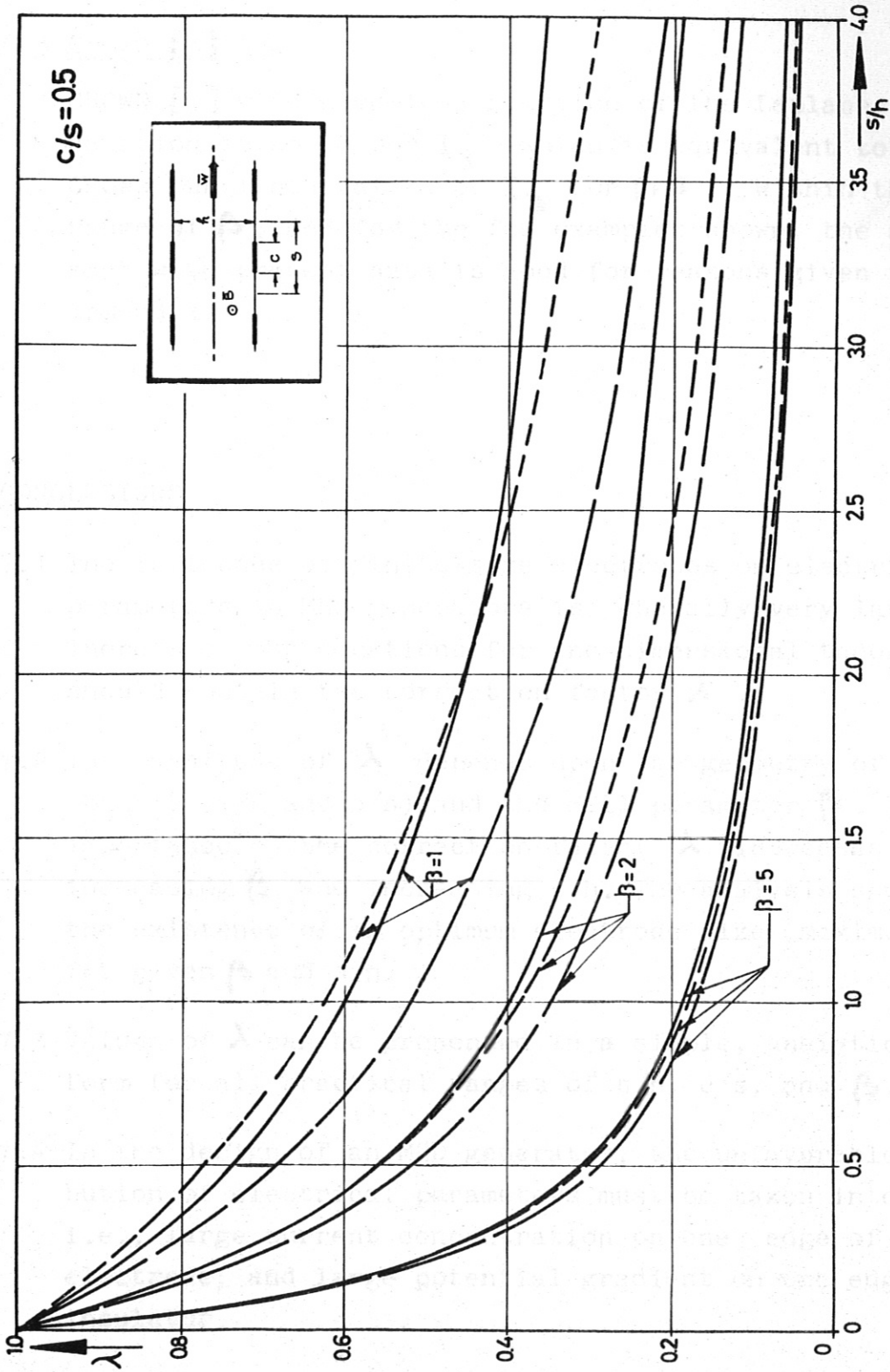


Fig. 38  $\lambda$  for  $c/s = 0.5$ , Comparison with Ref. [2]  
— Present analysis  
--- Ref. [2], exact values    - - - Ref. [2], approx. values

data, and a comparison on this basis is shown in Figure 39. The curves agree very well, except for some minor deviations which may be due to the difficulties of reading the published curve in Reference [4].

### 6.3 Crown [3]

CROWN [3] used numerical solution of the Laplace equation to solve for  $I_y$  (which is equivalent to  $1/\lambda$ ). CROWN published values of  $I_y$  for  $\beta \leq 2$ . Within this range of  $\beta$ , and for the few examples shown, the agreement with present data is good for reasons given in the Appendix.

## 7. CONCLUSIONS

- 7.1 The influence of finite-size electrodes on electrical parameters in MHD generators is generally very large. Therefore, the equations for one-dimensional theory should contain the correction factor  $\lambda$ .
- 7.2 The magnitude of  $\lambda$  depends upon the geometry of the channel ( $s/h$  and  $c/s$ ) and the Hall parameter  $\beta$ . The importance of the correction factor  $\lambda$  increases with increasing  $\beta$  and increasing  $s/h$ . The analysis shows the existence of an optimum electrode size (maximum  $\lambda$ ) for given  $\beta$  and  $s/h$ .
- 7.3 Values of  $\lambda$  can be presented in a simple, analytical form for all practical ranges of  $s/h$ ,  $c/s$ , and  $\beta$ .
- 7.4 In the design of an MHD generator, the unfavorable distribution of electrical parameters must be taken into account, i.e., large current concentration on one edge of the electrode, and large potential gradient on one edge of the insulator.

7.5 Consideration of electron heating in MHD generators must also take the distribution of electrical parameters into account. Potential drop near electrodes causes  $E_z$  in the channel, causing a steep gradient of ohmic losses across the channel. (The magnitude of the current concentration on one edge of the elec-

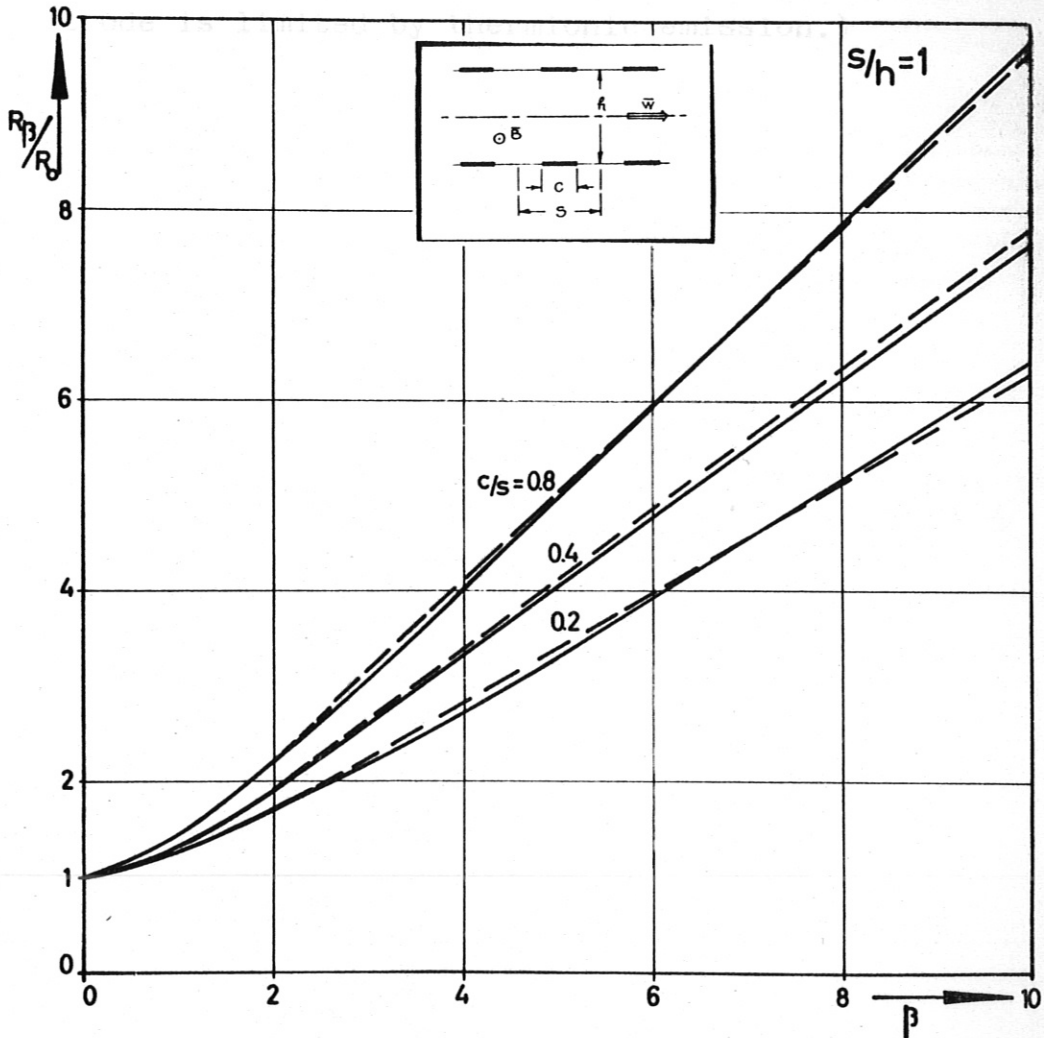


Fig. 39  $R_p/R_{p=0}$  for  $s/h = 1.0$ , Comparison with Ref. [4]  
 — Present analysis    -- Ref. [4]

A. APPENDIX

7.5 Considerations of electron heating in MHD generators must also take the distribution of electrical parameters into account. Potential drop near electrodes reduces  $E^*$  in the channel, causing a steep gradient of ohmic losses across the channel. (The magnitude of the current concentration on one edge of the electrode is limited by thermionic emission.)



Fig. A1.  $X/A$  for  $s/a = 0.5$ , Comparison with Ref. [3]

Fig. A1 shows a sample of the results of the analysis using Crown's method (Ref. [3]) and using the present method. In general, Crown's computation did converge for  $\beta \leq 2$ . For very small  $s/a$  values, convergence is achieved for  $\beta$ 's

A. APPENDIX

Computer Programming

An attempt to solve the Laplace equation for large Hall parameters using Crown's [3] approach was frustrated, because Crown's method did not lead to finite values of  $\gamma$ . The reason for the failure to obtain  $\gamma$  values for large  $\beta$  was found in the formulation of the boundary equation at the electrode. But only this equation has an influence on the distortion of the  $\gamma$ -field due to  $\beta$ , since only through this equation does  $\beta$  enter the calculation. Therefore, the boundary equation at the electrode was newly developed with the result that it is now applicable and correct for all  $\beta$ 's.

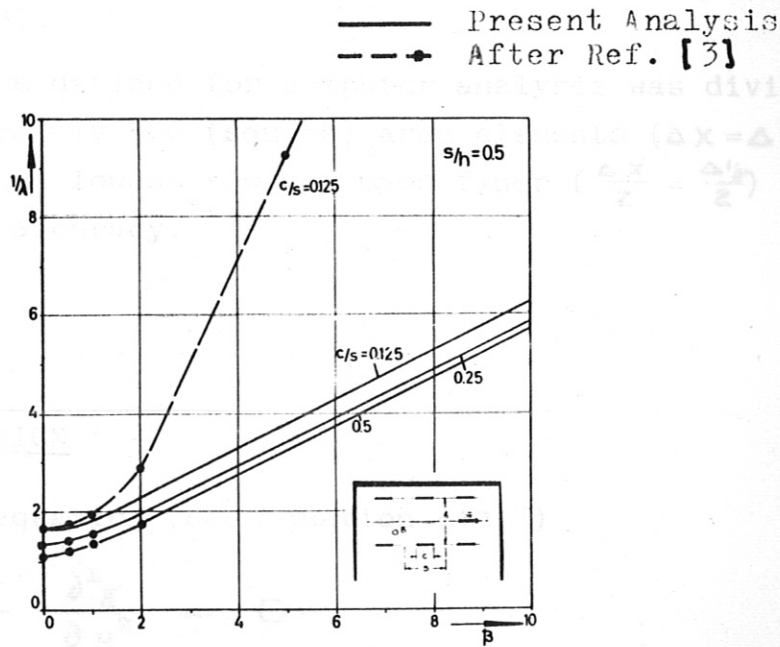


Fig. A.1  $\gamma/\lambda$  for  $s/h = 0.5$ , Comparison with Ref. [3]

Fig. A1 shows a sample of the results of the analysis using Crown's method (Ref. [3]) and using the present method. In general, Crown's computation did converge for  $\beta \approx 2$ . For very small  $c/s$  values, convergence is achieved for  $\beta$ 's

below 10. Crown's method and the present method lead to approximately the same results for  $\beta \approx 1$ . At  $\beta = 2$  the two methods still give almost identical answers for large  $c/s$ . But as  $c/s$  becomes smaller, the agreement between the two methods disappears.

### A.1 FIELD DESCRIPTION

The two-dimensional analysis of the MHD channel is performed with respect to the plane shown in Fig. A.2. This plane was limited to one section of the MHD generator because of periodicity of the electrical parameters (see Section 4.3.1). In the calculation, only the lower half of the plane shown was analyzed because of symmetry of generator phenomena (see Section 4.3.3).

The plane thus defined for computer analysis was divided into approximately 500 (square) area elements ( $\Delta x = \Delta y$ ). The mesh in the lowest row was made finer ( $\frac{\Delta x}{2} = \frac{\Delta y}{2}$ ) to obtain greater accuracy.

### A.2 LAPLACE EQUATION

The Laplace equation (see Equation (13) )

$$\frac{\partial^2 \gamma}{\partial x^2} + \frac{\partial^2 \gamma}{\partial y^2} = 0$$

can be written, for computer analysis, as a central-difference approximation of the second derivative:

$$\gamma_{m,n} = \frac{1}{4} [ \gamma_{m,n-1} + \gamma_{m+1,n} + \gamma_{m,n+1} + \gamma_{m-1,n} ] \quad (A.1)$$

In general, throughout the field of approximately 500 area elements, the values of  $\gamma$  vary slowly, so that the central-difference approximation should assure relatively good accuracy.

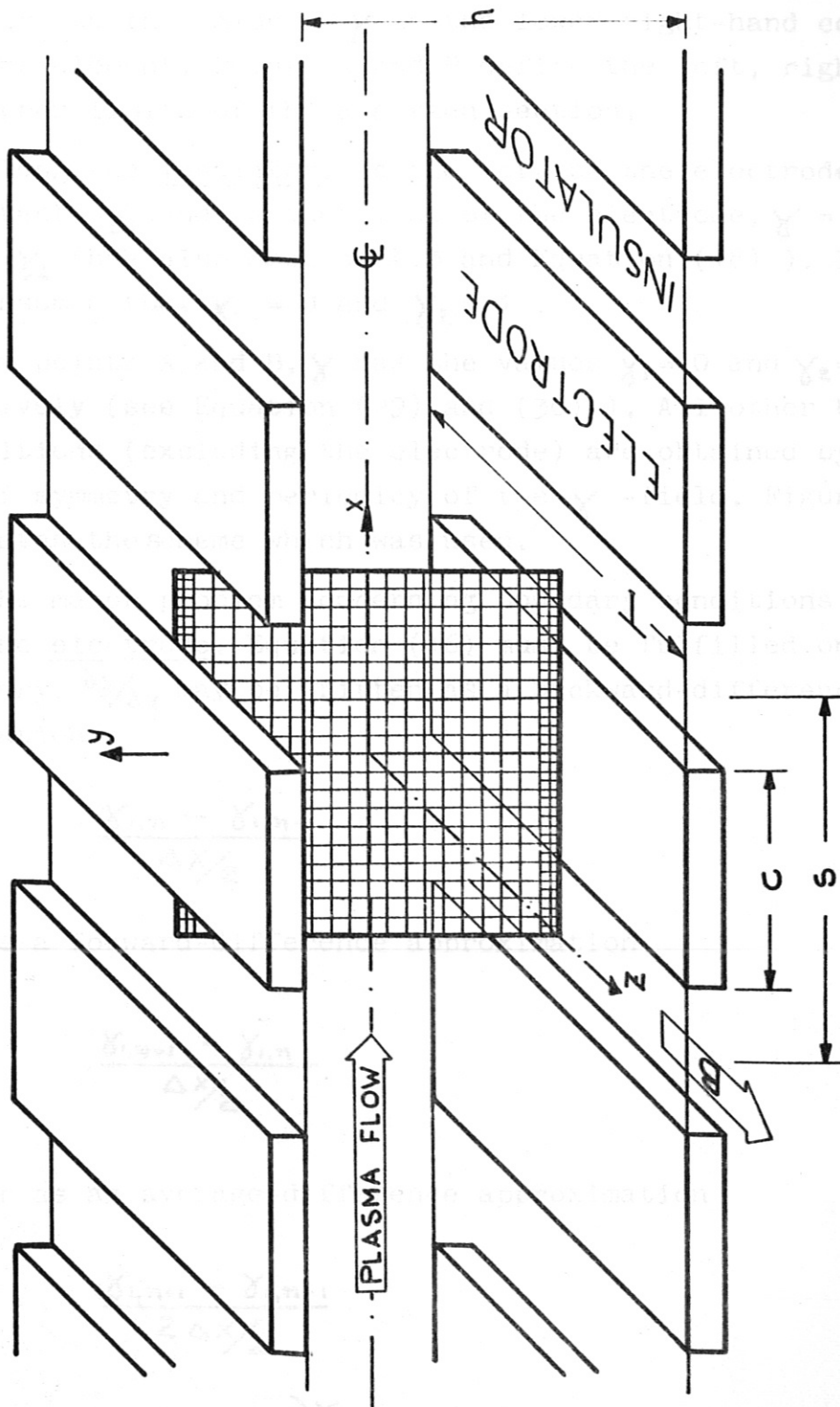


Fig. A.2 Channel Schematic



### A.3 BOUNDARY CONDITIONS

The scheme used to designate  $\gamma$  in each area element is shown in Fig. A.3. The  $\gamma$  written in each area element refers to the value of  $\gamma$  in the lower right-hand corner of the element. Points A and B define the left, right, and upper limits of the analyzed section.

Along the insulator, to the left of the electrode,  $\gamma = \text{constant} = \gamma_1$  and to the right of the electrode,  $\gamma = \text{constant} = \gamma_2$  (see also Section 4.3 and Equation (18)). It was assumed that  $\gamma_1 = 0$  and  $\gamma_2 = 1$ .

At points A and B,  $\gamma$  has the values  $\gamma_1 = 0$  and  $\gamma_2 = 1$ , respectively (see Equation (29) and (30)). All other boundary conditions (excluding the electrode) are obtained by making use of symmetry and periodicity of the  $\gamma$ -field. Figure A.3 indicates the scheme which was used.

The major problem concerning boundary conditions occurs on the electrode. Equation (16) must be fulfilled on this boundary.  $\frac{\partial \gamma}{\partial x}$  may be written as a backward-difference approximation

$$\frac{\gamma_{1,n} - \gamma_{1,n-1}}{\Delta x/2} \tag{A.2}$$

as a forward-difference approximation

$$\frac{\gamma_{1,n+1} - \gamma_{1,n}}{\Delta x/2} \tag{A.3}$$

or as an average-difference approximation

$$\frac{\gamma_{1,n+1} - \gamma_{1,n-1}}{2 \Delta x/2} \tag{A.4}$$

In equation (16),  $\frac{\partial \gamma}{\partial y}$  may be written as an upward-difference approximation

$$\frac{\gamma_{2,n} - \gamma_{1,n}}{\Delta y/2} \tag{A.5}$$

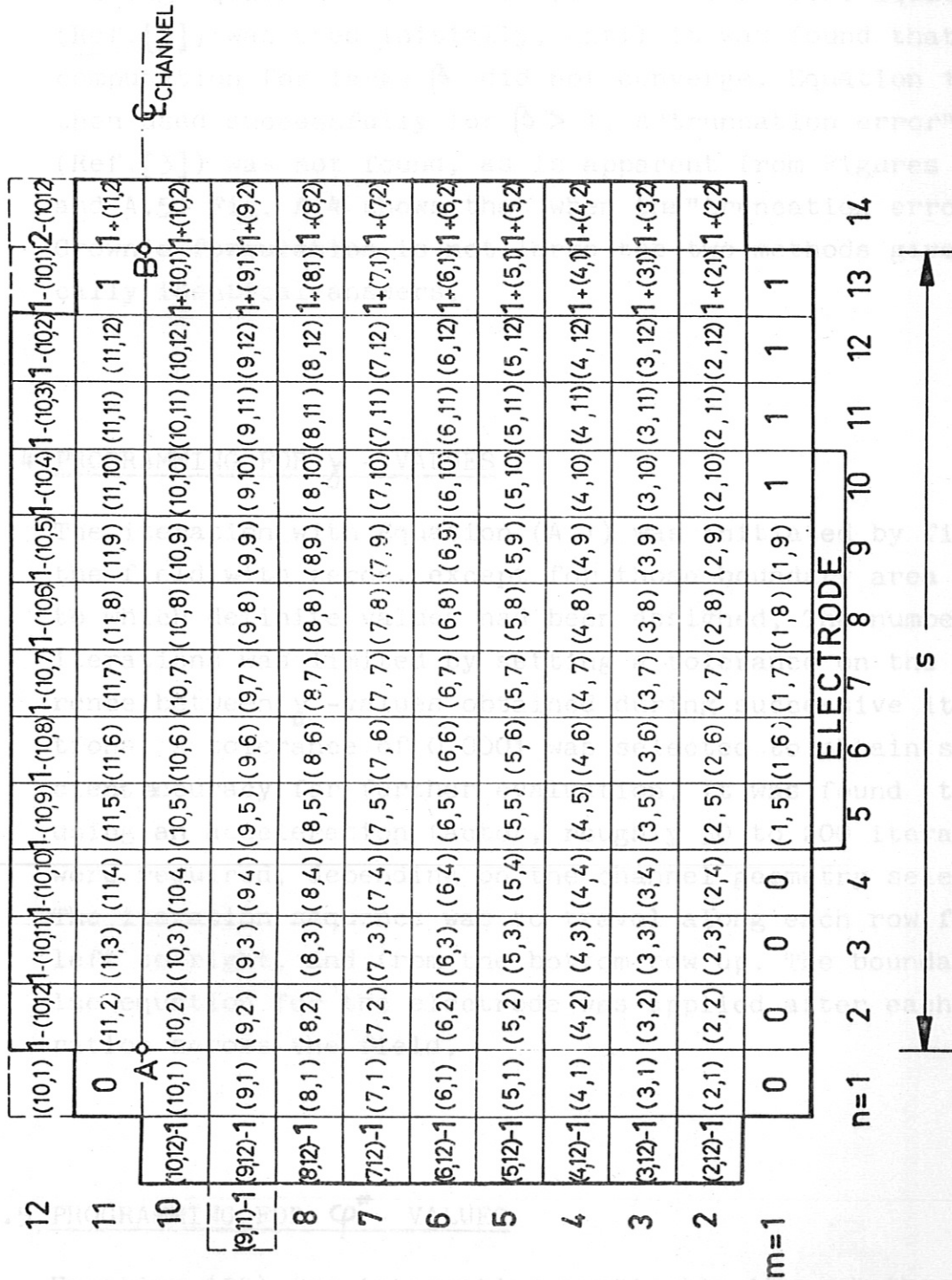


Fig. A.3 Schematic of Boundary Conditions for Computer Analysis  
 (In paranthesis are shown  $\gamma$  indices. Subdivision of row  $m=1$  is not shown.)

All other versions of writing  $\frac{\partial \gamma}{\partial y}$  will introduce an area element below the electrode which must be removed from the equation by means of the Laplace equation applied to the electrode surface. Table A.I shows six versions of writing equation (16) for computer calculation. Equation 6 (Ref.[3]) was used initially, until it was found that the computation for large  $\beta$  did not converge. Equation 1 was then used successfully for  $\beta > 1$ . A "truncation error" (Ref.[3]) was not found, as is apparent from Figures A.4 and A.5. Fig. A.4 shows that when the "truncation error" in Crown's formulation is not large the two methods give practically identical answers.

#### A.4 PROGRAMMING FOR $\gamma$ - VALUES

The iteration with Equation (A.1) was initiated by filling the field with zeros, except for those boundary area elements to which definite values had been assigned. The number of iterations was limited by setting a tolerance on the difference between  $\gamma$  -values obtained during successive iterations. A tolerance of 0.0001 was selected to obtain sufficient accuracy for further evaluation. It was found that, using an acceleration factor, roughly 50 to 200 iterations were required, depending on the channel geometry selected. The iteration sequence was to travel along each row from left to right, and from the bottom row up. The boundary value equation for the electrode was applied after each iteration across the field.

#### A.5 PROGRAMMING FOR $\varphi^*$ - VALUES

Equation (35) for integrating vertically through the field may be written

$$\varphi_{m,c}^* = \beta [\gamma_{m,c} - \gamma_{1,c}] + \frac{1}{2} \left[ \frac{\gamma_{m,c+1} - \gamma_{m,c-1}}{2} + \frac{\gamma_{1,c+1} - \gamma_{1,c-1}}{2} \right] + \sum_{m=2}^{m-1} \left( \frac{\gamma_{m,c+1} - \gamma_{m,c-1}}{2} \right) \quad (A.6)$$

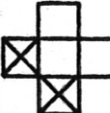
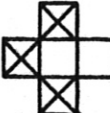
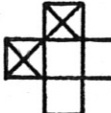
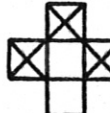
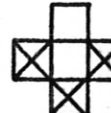
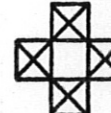
Eq. Scheme	$\chi_{i,n} =$	Remarks
1 	$\frac{\chi_{2,n} + \beta \chi_{1,n-1}}{1 + \beta}$	
2 	$\chi_{2,n} - \frac{\beta}{2} (\chi_{1,n+1} - \chi_{1,n-1})$	Divergent Iteration for $\beta \geq 2$
3 	$\frac{\chi_{2,n} - \beta \chi_{1,n-1}}{1 - \beta}$	Discontinuity at $\beta = 1$
4 	$\frac{\chi_{2,n} + (\frac{1}{2} - \beta) \chi_{1,n+1} + \frac{1}{2} \chi_{1,n-1}}{2 - \beta}$	Discontinuity at $\beta = 2$
5 	$\frac{\chi_{2,n} + \frac{1}{2} \chi_{1,n+1} + \frac{1}{2} (1 + 2\beta) \chi_{1,n-1}}{2 + \beta}$	
6 	$\frac{1}{2} \chi_{2,n} + \frac{1 - \beta}{4} \chi_{1,n+1} + \frac{1 + \beta}{4} \chi_{1,n-1}$	Divergent Iteration for $\beta \geq 3$

Table A.I

Electrode Boundary Equations

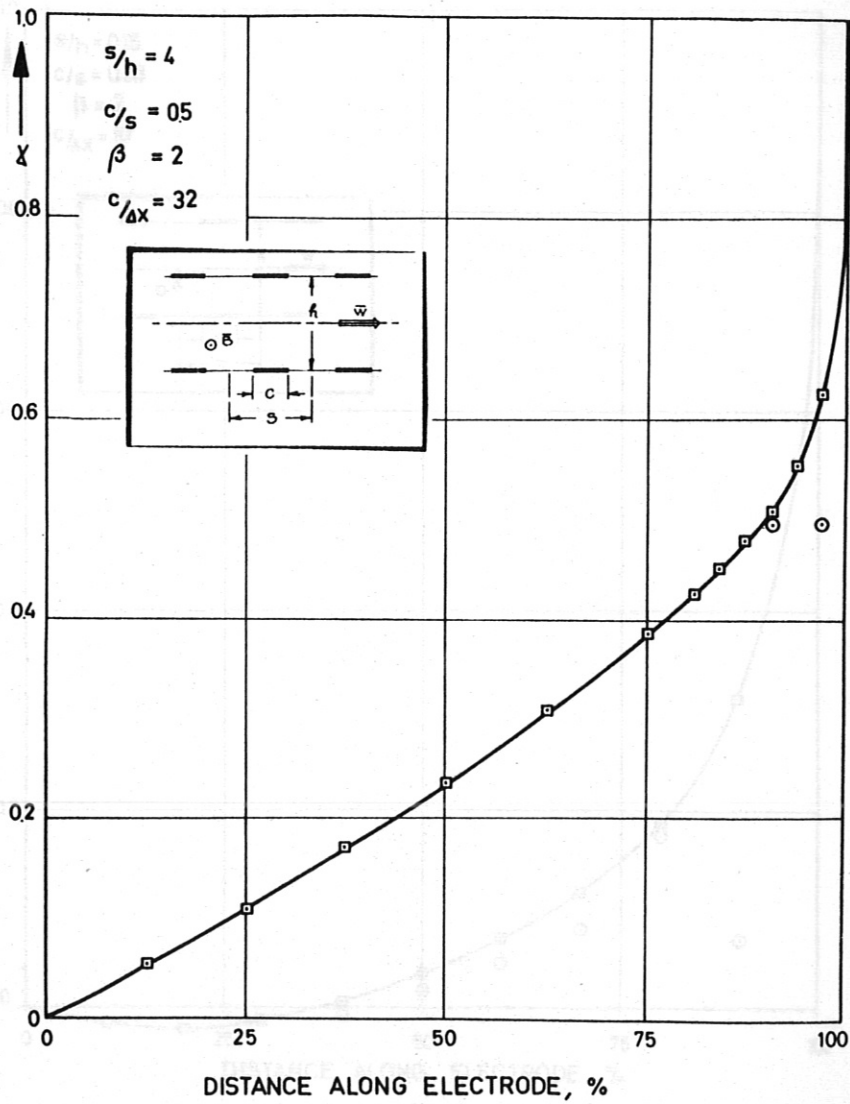


Fig. A.4  $\chi$  Along Electrodes for  $c/\Delta x = 32$   
Comparison with Ref. [3]  
□ Present analysis  
○ After Ref. [3]

Using the trapezoidal rule. In general,  $\psi^*$  varies sufficiently slowly in the field to permit the use of this approximate form of the integral.  $\gamma_{m,c}$  and  $\psi_{m,c}^*$  refer to  $\gamma$  and  $\psi^*$  values, respectively, along the perpendicular to the electrode at the electrode center. At the electrode surface,  $\psi_{m,c}^* = \psi_{m,c}$  is taken to zero (see Section 3).

Equation (37) for integrating horizontally through the field may be written

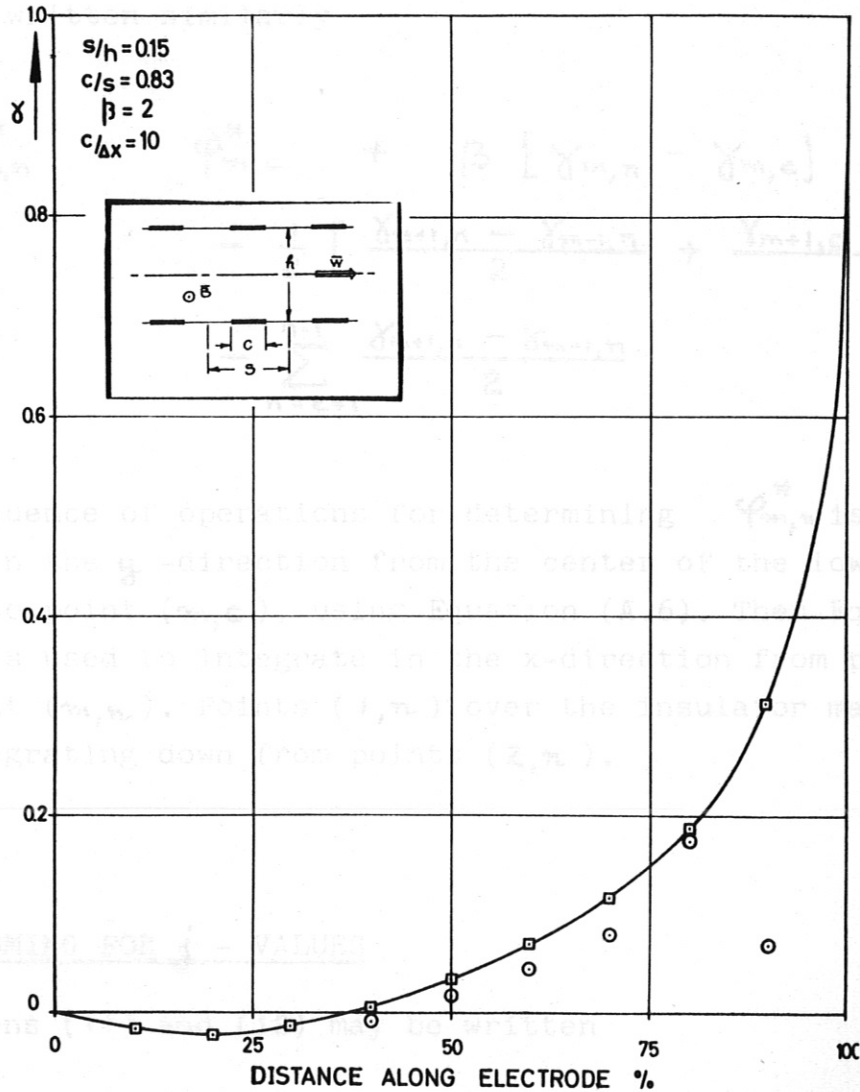


Fig. A.5  $\gamma$  Along Electrodes for  $c/\Delta x = 10$ , Comparison with Ref. [3]

- Present analysis
- After Ref. [3]

using the trapezoidal rule. In general,  $\varphi^*$  varies sufficiently slowly in the field to permit the use of this approximate form of the integral.  $\gamma_{m,c}$  and  $\varphi_{m,c}^*$  refer to  $\gamma$  and  $\varphi^*$  values, respectively, along the perpendicular to the electrode at the electrode center. At the electrode surface,  $\varphi_{m,c}^* = \varphi_{i,c}^*$  is taken as zero (see Section 5).

Equation (37) for integrating horizontally through the field may be written similarly

$$\begin{aligned} \varphi_{m,n}^* &= \varphi_{m,c}^* + \beta [\gamma_{m,n} - \gamma_{m,c}] \\ &\quad - \frac{1}{2} \left[ \frac{\gamma_{m+1,n} - \gamma_{m-1,n}}{2} + \frac{\gamma_{m+1,c} - \gamma_{m-1,c}}{2} \right] \\ &\quad - \sum_{n=c+1}^{n-1} \frac{\gamma_{m+1,n} - \gamma_{m-1,n}}{2} \end{aligned} \quad (A.7)$$

#### A.7 PROGRAMMING FOR OHMIC LOUDES

The sequence of operations for determining  $\varphi_{m,n}^*$  is to integrate in the  $y$ -direction from the center of the lower electrode to point  $(m,c)$ , using Equation (A.6). Then Equation (A.7) is used to integrate in the  $x$ -direction from point  $(m,c)$  to point  $(m,n)$ . Points  $(1,n)$  over the insulator may be found by integrating down from points  $(2,n)$ .

#### A.6 PROGRAMMING FOR $j$ - VALUES

Equations (11) and (12) may be written

$$j_x)_{m,n} = \frac{\partial \gamma}{\partial y} \Big|_{m,n} = \frac{1}{2\Delta y} (\gamma_{m+1,n} - \gamma_{m-1,n}) \quad (A.8)$$

and

$$j_z)_{m,n} = - \frac{\partial \gamma}{\partial x} \Big|_{m,n} = \frac{1}{2\Delta x} (\gamma_{m,n-1} - \gamma_{m,n+1}) \quad (A.9)$$

To determine  $j_x)_{m,n}$  along the insulator wall, use may be made

of Equations (5) and (36)

$$j_x)_{i,n} = \sigma_x E_x^*)_{i,n} = - \frac{\Delta \varphi^*}{\Delta x} )_{i,n} = \frac{\varphi_{i,n-1}^* - \varphi_{i,n+1}^*}{2 \Delta x} \quad (A.10)$$

The determine  $j_x)_{m,n}$  along the electrode wall, Equation (16) is applied

$$j_x)_{i,n} = - \beta j_y)_{i,n} \quad (A.11)$$

To make the j's comparable for differing field geometries, they are multiplied by s.

#### A.7 PROGRAMMING FOR OHMIC LOSSES

Values proportional to ohmic losses at each field point are found by simply adding the squared values of  $j_x)_{m,n}$  and  $j_y)_{m,n}$  for that point.

[1] Harris L.P., Cobine I.D.: The Significance of the Hall Effect in Three MHD (ASME Paper 60-WA-329, 1960)

[2] Harris L.P., Kill R.W.: Influence of Tensor Conductivity on Current Distribution in a MHD Generator (Journal of Applied Physics, 1961)

[3] Crown I.C.: Analysis of Magnetogasdynamic Generators Having Segmented Electrodes and Anisotropic Conductivity (United Aircraft Corporation, East Hartford, Conn., Report R-1652-2, February 1961)

[4] ... Characteristics of an MHD Generator with Finite Electrodes by Conformal Mapping under Full Consideration of Tensor Conductivity and a Velocity Profile (11. Intern. Symposium on MHD Electrical Power Generation, Paris, 6-11 July 1964)

[5] Yeh H., Sutton G.W.: Current Output and Efficiency of M.P.D. Generators with Segmented Electrodes and Non-Uniform Velocity Profiles (Symposium on MPD Electric Power Generation, Newcastle, September 1962)

[6] Louis I.F., Gal G., Blackburn P.R.: Detailed Theoretical and Experimental Study on a Large MHD Generator (5th Symposium on the Engineering Aspects of Magnetohydrodynamics, Massachusetts Institute of Technology, April 1964)



REFERENCES

- [1] Harris L.P., Cobine I.D.: The Significance of the Hall Effect in Three MHD Generator Configurations (ASME Paper 60-WA-329, 1960)
- [2] Hurwitz H., Kilb R.W., Sutton G.W.: Influence of Tensor Conductivity on Current Distribution in a MHD Generator (Journal of Applied Physics, Vo. 32, No 2, February 1961)
- [3] Crown I.C.: Analysis of Magnetogasdynamic Generators Having Segmented Electrodes and Anisotropic Conductivity (United Aircraft Corporation, East Hartford, Conn., Report R-1852-2, February 1961)
- [4] Schultz-Grunow F., Denzel D.L.: Calculation of the Electric Characteristics of an MHD Generator with Finite Electrodes by Conformal Mapping Under Full Consideration of Tensor Conductivity and a Velocity Profile (II. Intern. Symposium on MHD Electrical Power Generation, Paris, 6-11 July 1964)
- [5] Yeh H., Sutton G.W.: Current Output and Efficiency of M.P.D. Generators with Segmented Electrodes and Non-Uniform Velocity Profiles (Symposium on MPD Electric Power Generation, Newcastle, September 1962)
- [6] Louis I.F., Gal G., Blackburn P.R.: Detailed Theoretical and Experimental Study on a Large MHD Generator (5th Symposium on the Engineering Aspects of Magnetohydrodynamics, Massachusetts Institute of Technology, April 1964)

ACKNOWLEDGEMENT

The aid in computer programming by Mr. Ferd. Rehmet is gratefully acknowledged.